AD-A190 758 FLUID MOTION IN A SPINNING CONING CYLINDER VIA SPATIAL EIGENFUNCTION EXPANSION(U) ARMY BALLISTIC RESEARCH LAB ABERDEEN PROVING GROUND MD P HALL ET AL. AUG 87 1/1

UNCLASSIFIED BRL-TR-2813 F/G 20/4 NL

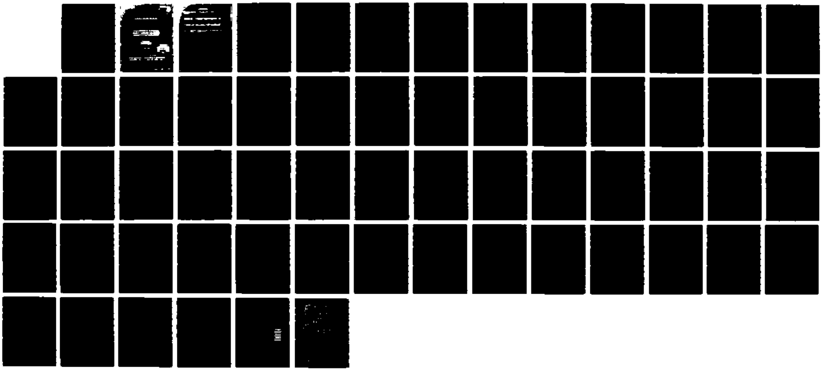

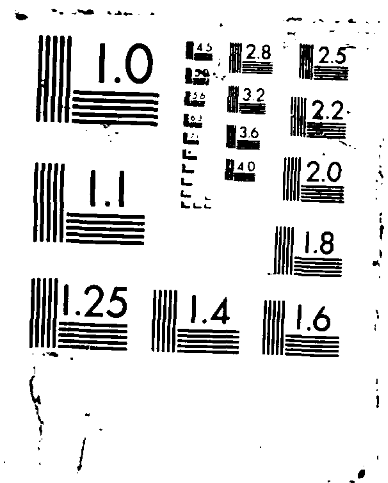
1.0
2.8
2.5
3.2
2.2
3.6
4.0
2.0
1.1
1.8
1.25
1.4
1.6

AD-A190 758

[illegible]

FLUID MOTION IN A [illegible] CONING C[illegible] EIGENFUNCTION [illegible]

[illegible]

AUGUST [illegible]

APPROVED FOR PUBLIC [illegible]

US ARMY BALLISTIC RESEARCH LABORATORY
ABERDEEN PROVING GROUND, MARYLAND

88 2 28 100

UNCLASSIFIED
SECURITY CLASSIFICATION OF THIS PAGE

AD-A190758

REPORT DOCUMENTATION PAGE

Form Approved
OMB No 0704-0188
Exp Date Jun 30, 1986

1a REPORT SECURITY CLASSIFICATION UNCLASSIFIED	1b. RESTRICTIVE MARKINGS
2a SECURITY CLASSIFICATION AUTHORITY 2b. DECLASSIFICATION / DOWNGRADING SCHEDULE	3. DISTRIBUTION / AVAILABILITY OF REPORT Approved for public release; distribution unlimited
4 PERFORMING ORGANIZATION REPORT NUMBER(S) BRL-TR-2813	5. MONITORING ORGANIZATION REPORT NUMBER(S)
6a. NAME OF PERFORMING ORGANIZATION U.S. Army Ballistic Research Laboratory 6b. OFFICE SYMBOL (If applicable) SLCBR-LF	7a. NAME OF MONITORING ORGANIZATION
6c. ADDRESS (City, State, and ZIP Code) Aberdeen Proving Ground, MD 21005-5066	7b. ADDRESS (City, State, and ZIP Code)
8a. NAME OF FUNDING / SPONSORING ORGANIZATION U.S. Army Ballistic Research Laboratory 8b OFFICE SYMBOL (If applicable) SLCBR-DD-T	9. PROCUREMENT INSTRUMENT IDENTIFICATION NUMBER
8c. ADDRESS (City, State, and ZIP Code) Aberdeen Proving Ground, MD 21005-5066	10. SOURCE OF FUNDING NUMBERS PROGRAM ELEMENT NO. 61102A PROJECT NO 1L161102AH43 TASK NO WORK UNIT ACCESSION NO

11. TITLE (Include Security Classification)
FLUID MOTION IN A SPINNING, CONING CYLINDER VIA SPATIAL EIGENFUNCTION EXPANSIONS

12. PERSONAL AUTHOR(S)
Hall,* Philip, Sedney, Raymond, and Gerber, Nathan

13a TYPE OF REPORT	13b TIME COVERED	14 DATE OF REPORT (Year, Month, Day)	15 PAGE COUNT
Technical Report	FROM ____ TO ____	1987 August	51

16. SUPPLEMENTARY NOTATION
This report supersedes IMR 886 dated April 1987.
**University of Exeter, Exeter, England, and ICASE, Hampton, Virginia

17 COSATI CODES			18. SUBJECT TERMS (Continue on reverse if necessary and identify by block number)	
FIELD	GROUP	SUB-GROUP	Liquid-Filled Projectile	Spatial Eigenvalues
01	01		Liquid Moment	Spectral Method
			Rotating Fluid	Spinning Nutating Cylinder

19. ABSTRACT (Continue on reverse if necessary and identify by block number) (bja)

The first attempts to explain the motion of a liquid-filled projectile were confined to the limit Reynolds Number = Re $\to \infty$ and linear theory. Recently, the need became apparent for the limit Re $\to 0$ for which the spatial eigenvalue method was developed; it is not restricted in Re, however. The eigenvalue problem is defined by ordinary differential equations in the radial direction. The eigenvalues are determined by an iterative process for which sufficiently accurate initial estimates are required. The flow variables are expanded in an eigenfunction series with coefficients determined by satisfying the boundary conditions; a least squares method and collocation method are used for this purpose. The

(continued)

20 DISTRIBUTION / AVAILABILITY OF ABSTRACT ☐ UNCLASSIFIED/UNLIMITED ☒ SAME AS RPT ☐ DTIC USERS	21 ABSTRACT SECURITY CLASSIFICATION UNCLASSIFIED
22a NAME OF RESPONSIBLE INDIVIDUAL Raymond Sedney	22b TELEPHONE (Include Area Code) (301)-278-3816 22c OFFICE SYMBOL SLCBR-LF

19. ABSTRACT (continued)

pressure and shear stress so determined give the pressure coefficient and overturning moment. The accuracy of the calculation is discussed. Results are given over a range of Re, aspect ratio, and nutational frequency. The CPU time required on the VAX 8600 varies from 10 seconds at Re = 10 to 30 minutes at Re = 1,000. Results are compared with experimental measurements. Comparisons are also made with results from the large scale finite difference program of Strikwerda.

ACKNOWLEDGMENTS

We thank Mr. William H. Mermagen, U.S. Army Ballistic Research Laboratory (BRL), Launch and Flight Division, Aberdeen Proving Ground, Maryland, for his helpful conversations on this problem and his considerable help in getting several programs operational.

Accession For
NTIS GRA&I ☒
DTIC TAB ☐
Unannounced ☐
Justification
By
Distribution/
Availability Codes

Dist	Avail and/or Special
A-1	

DTIC COPY INSPECTED 1

TABLE OF CONTENTS

LIST OF FIGURES

LIST OF FIGURES (continued)

I. INTRODUCTION

For many years it has been observed that liquid-filled projectiles have a proclivity for unusual flight behavior, often being unstable even though the same projectile with a solid payload is stable. The history of various aspects of this area of ballistics, summaries and critiques of previous theoretical work and a discussion of experimental techniques are given in References 1 and 2. The distinction between the steady state and spin-up problems is basic.[1,2] Only the steady state problem for an incompressible fluid in a cylinder is considered here; therefore, the undisturbed basic flow is solid body rotation. In principle, the same techniques could be used for the spin-up problem.

To put this work in perspective, it is helpful to distinguish between analytical and finite difference approaches (see References 1 and 2). So far, analytical approaches have been confined to linearized problems. Most of these are asymptotic for Re $\to \infty$; the case Re $\to 0$ was considered by Sedney (unpublished, see Reference 1 for a summary). The Reynolds number, Re, is defined below. Herbert[3] analyzed experimental data at "low Re" and constructed a model for an infinite cylinder from which he deduced results for $1 \leq \mathrm{Re} \leq 10^4$. His results for roll moment agree with experiment. In principle, the analytical approach used in this work is valid for all Re; it is "exact" in the sense that the accuracy of the results can be improved by adding more eigenfunctions in the expansion. In practice, treating large Re, say Re $\geq$ 1,000, becomes tedious using the techniques presented here.

An outline of the process in going from the Navier-Stokes equations to the linear partial differential equations and the boundary conditions is given now; the details are in Reference 4.

1. The Navier-Stokes equations are written in an inertial reference frame using cylindrical polar coordinates (r,θ,x) with corresponding velocity components (u,v,w); an inertial frame is used even though there is an advantage to using an aeroballistic reference frame in that the boundary conditions are easier to apply (see Reference 1).

2. To obtain boundary conditions, the motion of the cylinder walls is determined from the projectile motion which is proportional to $\exp i(ft-\theta)$ where t is time and f is, in general, the non-dimensional complex frequency of the projectile motion; for convenience, f is taken to be real here, so that $f = \tau$, the non-dimensional coning frequency for pure coning motion.

3. The angle of the coning motion, K_0, is assumed small and only linear departures from solid body rotation are considered. The velocity components are then $(-K_0\, u^*,\ r - K_0\, v^*,\ -K_0\, w^*)$ and pressure is $1/2\ r^2 - K_0\, p^*$. The * denotes perturbation.

4. The motion of the cylinder is specified and the response of the fluid determined; no feedback from the fluid to the projectile is allowed.

5. It is convenient to introduce complex velocities and pressure, denoted by sub _ and defined by

$$(u^*,v^*,w^*,p^*) = \text{Real}\left\{(\underline{u},\underline{v},\underline{w},\underline{p}) \exp i(ft-m\theta)\right\} \tag{1.1}$$

where the azimuthal wave number, m, is an integer (±) but only m = 1 is needed for the linear forced motion problem.

The resulting linearized, non-dimensional Navier-Stokes equations are:

$$i(f-m)\,\underline{u}-2\underline{v} = -\underline{p}_r + Re^{-1}\left[\nabla^2\underline{u} - \frac{m^2+1}{r^2}\underline{u} + \frac{2\,im}{r^2}\underline{v}\right]$$

$$i\,(f-m)\,\underline{v} + 2\underline{u} = (im/r)\,\underline{p} + Re^{-1}\left[\nabla^2\underline{v} - \frac{m^2+1}{r^2}\underline{v} - \frac{2\,im}{r^2}\underline{u}\right]$$

$$i\,(f-m)\,\underline{w} = -\underline{p}_x + Re^{-1}\left[\nabla^2\underline{w} - \frac{m^2}{r^2}\underline{w}\right]$$

$$(r\underline{u})_r - im\,\underline{v} + r\underline{w}_x = 0\ , \tag{1.2a,b,c,d}$$

where $\nabla^2 = \partial_r{}^2 + (1/r)\,\partial_r + \partial_x{}^2$ is the Laplacian and subscripts denote partial derivatives. The non-dimensional variables are defined after (2.1).

From (1.2) and appropriate boundary conditions, the eigenvalue and forced motion problems are defined in Section II. Particular solutions of the partial differential equations which simplify application of boundary conditions are also introduced there, and finally, the eigenfunction expansion of the solution. The latter is the basis of the spatial eigenvalue method which was used by Blennerhasset and Hall[5] in their study of the Taylor vortex problem for finite length cylinders.

Methods for solving the eigenvalue problem are discussed in Section III. Obtaining the eigenvalues is central to the method and is a nontrivial problem. The complex eigenvalues are defined by a 6th order complex system of ordinary differential equations which is not self-adjoint and are computed by an iterative process. Sufficiently accurate initial estimates, or first guesses, are required for the iteration process to converge; these are obtained using asymptotic approximations for $Re \to 0$ and $Re \to \infty$, variation on the axisymmetric Taylor problem for Re not too large, or extrapolation. Additionally, an algorithm was developed to compute an initial estimate from a previous eigenvalue by a trivial arithmetic operation. Once the eigenvalues and eigenfunctions are known, the coefficients in the expansion must be computed; collocation and least squares methods are used.

Formulas for pressure and moment coefficients are presented and discussed in Section IV. Asymptotic forms for the pressure coefficient for $f \to 0$ and $f \to \infty$ are also given.

Results are presented in Section V. Although the velocities and pressure are available in the output, they are usually not extracted. Instead, the variation of pressure and moment coefficients with Re, f or aspect ratio are shown since these are the items of primary interest. Some comparisons are made with results from experiments. Several comparisons are also made with results from the finite difference method of Strikwerda,[6] as computed by Nusca.[7] Rather limited comparisons are made with results from other numerical methods.

Because of the emphasis given results from the Strikwerda[6] method in Section V, it is apropos to consider some features of it. Since it solves the nonlinear Navier-Stokes equations, it can handle large K_0; and it computes both the roll and side moment coefficients. At present, it has been applied to Re $\leq$ 100, Reference 7. CPU time on the VAX 8600 is of the order of hours, increasing with Re. For example, if Re = 10, f = 0.05, and aspect ratio (length/diameter) of the cylinder is 3.0, it is 1.1 hours.

The spatial eigenvalue method is in the class of spectral methods; it is applied here only to the linear problem (extension to the nonlinear case is underway). Thus, K_0 must be small in some sense. Although the spatial eigenvalues method was intended originally for application to the "small" Re range, say Re $\leq$ 100, which is the range emphasized in this report, in principle it can be applied to any Re; actually only Re $\leq$ 1000 has been considered. The CPU time on the VAX 8600 is of the order of minutes, increasing with Re; for Re = 10, f = 0.05 and aspect ratio = 3.0, it is 10 seconds if 6 eigenvalues are used (with a maximum of 4 iterations) and 30 seconds if 15 eigenvalues are used (with a maximum of 8 iterations). The side moment coefficients computed with 6 or 15 eigenvalues differ by 0.15% for this case. For Re = 1000 and f = 0.1, the CPU time is approximately 30 minutes.

II. FORMULATION OF THE PROBLEM

Consider the flow of a viscous fluid of kinematic viscosity ν and density ρ in a circular cylinder of radius a and length 2c. The aspect ratio is $A \equiv c/a$. The undisturbed fluid is assumed to be in rigid body rotation with angular velocity Ω, as observed in an aeroballistic reference frame, S'; see Reference 6, e.g. With respect to the inertial reference frame, S, used here the angular velocity is $\Omega + \bar{\tau} \cos K_0$, about the x-axis, where $\bar{\tau}$ is the dimensional coning frequency; it is used to define the Reynolds number

$$Re = (\Omega + \bar{\tau} \cos K_0)\, a^2/\nu \,. \qquad (2.1)$$

In S' the non-dimensional coning frequency is $\tau' = \bar{\tau}/\Omega$ and the Reynolds number is $Re' = \Omega a^2/\nu$. For reference, in S the non-dimensional coning frequency is $f = \tau = \tau'/(1 + \tau' \cos K_0)$ and $Re = Re'/(1 - \tau \cos K_0)$. Using the assumption already introduced, $K_0 \ll 1$, $\cos K_0$ is replaced by unity in the above and the following. The typical time, length, velocity, and pressure scales used to non-dimensionalize the flow variables are $(\Omega + \bar{\tau})^{-1}$, a, $(\Omega + \bar{\tau})a$ and $\rho a^2(\Omega + \bar{\tau})^2$.

As for any oscillatory system two problems are defined: the free oscillation or eigenvalue problem and the forced oscillation problem here called the moment problem. For the eigenvalue problem, the complex perturbation velocities and pressure in (1.1) are written

$$(\underline{u},\underline{v},\underline{w},\underline{p}) = U(r)\sin Kx,\ V(r)\sin Kx,\ W(r)\cos Kx,\ P(r)\sin Kx \quad . \tag{2.2}$$

From (1.2) the radial variations (U,V,W,P) satisfy

$$[Re^{-1}(\Delta_1 - r^{-2}) - iM]\,U + 2\,[1 + (im/r^2\,Re)]\,V - P_r = 0$$

$$[Re^{-1}(\Delta_1 - r^{-2}) - iM]\,V - 2[1 + (im/r^2\,Re)]\,U + \frac{im\,P}{r} = 0$$

$$[Re^{-1}\,\Delta_1 - iM]\,W - KP = 0$$

$$(rU)_r - imV - KrW = 0 \ . \tag{2.3a,b,c,d}$$

where $M = f - m$,

and $\Delta_1 \equiv \partial_{rr} + \frac{1}{r}\partial_r - [\frac{m^2}{r^2} + K^2]$.

See also Reference 8 for these equations in a different context. The above equations must be solved subject to the no-slip condition at $r = 1$, $U = V = W = 0$, together with the appropriate boundary conditions at $r = 0$, which depend on m and can be written

$$U = V = \frac{dW}{dr} = 0, \qquad m = 0$$

$$U - iV = W = P = 0, \qquad m = 1$$

$$U = V = W = 0, \qquad m > 1. \tag{2.4a,b,c}$$

For a discussion of the origin of these boundary conditions, see Batchelor and Gill[9] and Reference 4. The system (2.3), the no-slip condition at $r = 1$ and one of (2.4) constitute an eigenvalue problem for $K = K(m,Re,f)$. Since the problem is defined on a finite interval, it is expected that the spectrum will be infinite and discrete. If neutral disturbances were possible, then K would, of course, be real. The numerical solution of the eigenvalue problem is discussed in the next section; here it is assumed that an infinite sequence of eigenvalues $\{K_n\}$ exists and can be ordered in some sensible manner.

For the moment problem, it can be shown that only m = 1 is required. The pivot point for the coning motion is midway along the axis of the cylinder ($\ell = 0$ in the notation of Reference 4). The boundary conditions at r = 1 and $x = \pm A$ for $(\underline{u},\underline{v},\underline{w})$ were derived in Reference 4; they are

$$\underline{u} = -i\ (1 - f)\ x$$

$$\underline{v} = -(1 - f)\ x$$

$$\underline{w} = i\ (1 - f)\ r\ . \qquad (2.5a,b,c)$$

It is convenient at this stage to transfer the inhomogeneous boundary conditions to the endwalls by subtracting out a suitable particular solution to the perturbed Navier-Stokes equations. Let

$$\underline{u} = -i\ [1 - f]\ x + u\ (r,x)$$

$$\underline{v} = -[1 - f]\ x + v\ (r,x)$$

$$\underline{w} = i\ [1 - f]\ r + \sigma(r) + w\ (r,x)$$

$$\underline{p} = -[1 - f^2]\ rx + p\ (r,x)$$

$$\sigma(r) = 2if\ [r - \frac{J_1(\lambda r)}{J_1(\lambda)}] \qquad (2.6a,b,c,d,e)$$

where J_1 is the Bessel function of the first kind and order 1 and $\lambda = (1 + i)\ [(1 - f)\ Re/2]^{1/2}$. The boundary conditions at r = 0,1 and $x = \pm A$ in terms of (u,v,w,p) become

$$u - iv = w = p = 0, \qquad r = 0$$

$$u = v = w = 0, \qquad r = 1$$

$$u = v = 0,\ w = -\sigma(r) \qquad x = \pm A \qquad (2.7a,b,c)$$

and the differential equations satisfied by (u,v,w,p) are (1.2) with $m = 1$:

$$i\,[f - 1]\,u - 2v = -p_r + \frac{1}{Re}\left\{\nabla^2 u - \frac{2u}{r^2} + \frac{2iv}{r^2}\right\},$$

$$i\,[f - 1]\,v + 2u = \frac{ip}{r} + \frac{1}{Re}\left\{\nabla^2 v - \frac{2v}{r^2} - \frac{2iu}{r^2}\right\},$$

$$i\,[f - 1]\,w = -p_x + \frac{1}{Re}\left\{\nabla^2 w - \frac{w}{r^2}\right\},$$

$$(ru)_r - iv + rw_x = 0 \,. \qquad (2.8a,b,c,d)$$

Assuming that $(u,v,p) = (U(r),\ V(r),\ P(r))\sin Kx$ and $w = W(r)\cos Kx$, it follows that U,V,W,P satisfy (2.3) with $m = 1$; the odd and even variations with x follow from (2.5) and (2.6). Let the infinite sequence of eigenvalues, $\{K_n\}$, with $m = 1$ be denoted by $\{k_n\}$ and the eigenfunctions by u_n, v_n, w_n, p_n. The solution of (2.8) is expressed as an eigenfunction expansion:

$$u = \sum_{n=1}^{\infty} \frac{\alpha_n \sin k_n x}{\sin k_n A}\, u_n(r), \qquad v = \sum_{n=1}^{\infty} \frac{\alpha_n \sin k_n x}{\sin k_n A}\, v_n(r),$$

$$w = \sum_{n=1}^{\infty} \frac{\alpha_n \cos k_n x}{\sin k_n A}\, w_n(r)\,, \qquad p = \sum_{n=1}^{\infty} \frac{\alpha_n \sin k_n x}{\sin k_n A}\, p_n(r)\,. \qquad (2.9a,b,c,d)$$

Discussions of how $\{k_n\}$ can be sensibly ordered and how the as yet undetermined constants $\{\alpha_n\}$ can be found, by applying the endwall boundary conditions, are given in the next section.

III. CALCULATION OF THE EIGENVALUES AND SERIES COEFFICIENTS

The first step in the calculations is to find $\{k_n\}$ and $\{u_n, v_n, w_n, p_n\}$, the eigenvalues and eigenfunctions of (2.3) with $m = 1$, subject to

$$u_n - iv_n = w_n = p_n = 0, \qquad r = 0,$$

$$u_n = v_n = w_n = 0, \qquad r = 1. \qquad (3.1a,b)$$

Two independent methods were used to generate the eigenvalues; since both iterative methods are well documented elsewhere, only a brief description of them is given.

Firstly, the complete orthonormalization procedure of Davey,[10] as implemented by Kitchens, Gerber, and Sedney[11] was employed. The numerical integration was carried out using a fourth order Runge-Kutta scheme. Secondly, the compact finite difference scheme of Malik, Chuang, and Houssaini[12] was used. In both methods the singularity in the equations at $r = 0$ was removed by transferring the boundary conditions to $r = \varepsilon$ with $0 < \varepsilon << 1$ and using the Taylor series solution given in Reference 11. The methods gave consistent results. The complete orthonormalization method was more efficient at Reynolds number of order 10^2. At higher Reynolds numbers where some of the eigenfunctions begin to vary rapidly, the finite difference method was found to be the more efficient method.

With both methods a sufficiently accurate guess for k_n was required if the iterations were to converge. This was a hindrance initially since little previous knowledge of the distribution of these eigenvalues was available; in certain cases it was necessary to calculate a large number of the sequence $\{k_n\}$. To obtain first guesses techniques were developed to determine approximations to the eigenvalue distribution in certain special limits, and if necessary, follow their evolution into the required regime.

1. A RELATED TAYLOR VORTEX PROBLEM.

Firstly, previous knowledge of the eigenvalue distribution for the classical Taylor vortex problem was used (see Reference 5). Consider a basic flow driven by the rotation of the cylinder $r = \varepsilon$ while the outer cylinder is held fixed. No-slip boundary conditions are applied at $r = \varepsilon$ and at $r = 1$. The frequency, f, and azimuthal wave numbers, m, are now set to zero; at sufficiently small supercritical Reynolds numbers the resulting eigenvalue distribution is as sketched in Figure 1. The two real wave numbers k_1 and k_2 correspond to the two neutrally stable perturbations which exist in this regime. In addition, there are the following three sets of eigenvalues:

(1) A pure imaginary set $\{k_{3n}\}$, $n = 1,2,...$

(2) A complex set of eigenvalues $\{k_{3n+2}\}$, $n = 1,2,...$
with $k_{3n+2} = \bar{k}_{3n+1}$,

(3) A complex set of eigenvalues k_{3n+1}, $n = 1,2,...$
being in the first quadrant with real part $\sim \pi$.

The eigenvalues k_1 and k_2 can be associated with (3) and (2), respectively, and at subcritical Reynolds numbers move into the complex plane with $k_1 = \bar{k}_2$.

At higher Reynolds numbers pairs of eigenvalues (k_{3n+1}, k_{3n+2}) merge on the real axis and then move along the real axis. Blennerhasset and Hall[5] found that the eigenvalues $\{k_{3n+1}, k_{3n+2}, k_{3n+3}\}$ for n = 0,1,2, have azimuthal velocity eigenfunctions with n zeros in (ε,1). Thus, in the axisymmetric problem, there is a rational method of ordering the eigenvalues, in triplets. If m or f is now taken to be nonzero, the symmetry of the eigenvalue distribution described above is broken but the ordering from the axisymmetric steady Taylor vortex problem can be retained while:

a. f and m are gradually increased from zero to their required values.

b. The basic flow is gradually varied from that appropriate to the Taylor problem to rigid body rotation.

c. The boundary conditions at $r = \varepsilon$ are gradually varied from no-slip to those given by the Taylor series expansion of Reference 11.

It was found that it was not necessary to perform a, b, and c independently and that having found a set of eigenvalues $\{k_n\}$ for some f and Re, other sets could be generated by varying f and/or Re slowly, i.e., by extrapolation. However, at values of Re greater than about 100, the eigenvalues (2) and (3) were found to be very sensitive to changes in Re and it proved rather inefficient to calculate them by this method. For large Re an asymptotic approach was used, described below. Another asymptotic approach, for small Re, is necessary and outlined next.

2. Re $\rightarrow$ 0.

For values of Re $\lesssim$ 10, approximately, estimates for the eigenvalues can be found by solving the Re $\rightarrow$ 0 problem, i.e., the Stokes limit. Essentially, the same procedure is used as for the classical Stokes flow solution but Re $\rightarrow$ 0 is a regular perturbation for the internal flow under consideration. In addition to the momentum and continuity equations, (2.8), a derived equation is used. The linearized Navier-Stokes momentum equations, in vector form with velocity vector $q^* = (u^*,v^*,w^*)$, see (1.1), can be written

$$i(f - 1)\, q^* + 2\,(i_x \times q^*) = -\text{grad}\, p^* - (1/Re)\, \text{curl}\, \omega^*$$

where ω^* is vorticity and i_x is the unit vector in the x direction. Using div q^* = div curl ω^* = 0 and the definitions (1.1) yields

$$r\,[\nabla^2 \underline{p} - \underline{p}/r^2] = 2\,[i\underline{u} + (r\underline{v})_r]\,. \qquad (3.2)$$

Next, the scaled pressure $\tilde{P} = \underline{p}\, Re$ is introduced and it is convenient to change variables u and v to $\tilde{U} = u + iv$ and $\tilde{V} = u - iv$. A regular perturbation series

$$(\tilde{U},\tilde{V},w,\tilde{P}) = \sum_{j=0}^{\infty} (\tilde{U}_j,\ \tilde{V}_j,\ w_j,\ \tilde{P}_j)\ Re^j$$

is substituted into (2.8), (3.2), and (2.7) and the latter is expanded in a power series in Re. The result is

$$\nabla^2 \tilde{U}_j = \tilde{P}_{jr} + \tilde{P}_j/r$$

$$\nabla^2 \tilde{V}_j - (4/r^2)\ \tilde{V}_j = \tilde{P}_{jr} - \tilde{P}_j/r$$

$$\nabla^2 w_j - (1/r^2)\ w_j = \tilde{P}_{jx}$$

$$\tilde{U}_{jr} + \tilde{V}_{jr} + (2/r)\ \tilde{V}_j + 2\ w_{jx} = 0$$

$$\nabla^2 \tilde{P}_j - (1/r^2)\ \tilde{P}_j = 0\ . \qquad (3.3a,b,c,d,e)$$

Using the expanded boundary conditions (2.7), the trivial solution is obtained for the O(1) terms. The O(Re) solution is determined from homogeneous and non-homogeneous solutions of (3.3), with respect to $\tilde{P}_1$. Expressing the O(Re) terms as a modal decomposition, as in (2.2),

$$(\tilde{U}_1,\tilde{V}_1,w_1,\tilde{P}_1) = \ F_n(r)\ \sin\lambda_n x,\ G_n(r)\ \sin\lambda_n x,\ H_n(r)\ \cos\lambda_n x,\ \Pi_n(r)\ \sin\lambda_n x\ ,$$

the eigenfunctions are found to be

$$F_n = [r\ J_0(\Lambda_n)\ J_1\ (\Lambda_n r) - J_1\ (\Lambda_n)\ J_0\ (\Lambda_n r)]/J_0\ (\Lambda_n)$$

$$G_n = [r\ J_2\ (\Lambda_n)\ J_1\ (\Lambda_n r) - J_1\ (\Lambda_n)\ J_2\ (\Lambda_n r)]/J_2\ (\Lambda_n)$$

$$H_n = i\ [r\ J_1\ (\Lambda_n)\ J_0\ (\Lambda_n r) - J_0\ (\Lambda_n)\ J_1\ (\Lambda_n r)]/J_1\ (\Lambda_n)$$

$$\Pi_n = 2\ J_1\ (\Lambda_n r) \qquad (3.4a,b,c,d)$$

where $\Lambda_n = i\lambda_n$, are the roots of

$$\Lambda_n\ J_1^2\ (J_0 - J_2) - 2\ \Lambda_n\ J_0^2\ J_2 - 2\ J_0\ J_1\ J_2 = 0\ . \qquad (3.5)$$

Obviously, the λ_n do not depend on any of the parameters of the problem; the first several λ_n are shown in Figure 2, indicated by k_n since $\lambda_n = \lim_{Re \to 0} k_n$. These eigenvalues separate into three branches or sets:

(1) a set which is pure imaginary,

(2) a set in the fourth quadrant, and

(3) a set which is conjugate to (2).

As an alternate notation for the λ's or k's, let the eigenvalues be denoted by $\lambda_{\ell,n}$ where $\ell = 1,2,3$ is the branch and $n = 1,2,...$ is the index along a branch. If $j_{0,n}$ and $j_{2,n}$ are the n-th zeroes of J_0 and J_2, respectively,

$$\lambda_{1,n} \sim i\,(j_{0,n+2} + j_{2,n})/2$$

for $n \gg 1$. This asymptotic estimate is quite accurate for $n \geq 1$. From this $\lambda_{1,n+1} - \lambda_{1,n} \approx i\pi$. Actually, the eigenvalues for finite Re satisfy $\mathrm{Im}\,(k_{\ell,n+1} - k_{\ell,n}) \approx \pm\pi$, + for $\ell = 1,3$ and - for $\ell = 2$, for all ℓ and Re if $n \geq n_0(Re)$. The relationship $n_0(Re)$ is only known empirically. An algorithm for obtaining a first guess for $k_{\ell,n}$ is:

For given ℓ, Real $k_{\ell,n}$ is obtained by extrapolating Real $k_{\ell,n-2}$ and

Real $k_{\ell,n-1}$, and $\mathrm{Im}\,(k_{\ell,n} - k_{\ell,n-1}) = \pm\pi$ for $n \geq n_0$.

The $k_{\ell,n}$ were computed up to Re = 100, starting from the $\lambda_{\ell,n}$, by slowly increasing Re and using the algorithm. Relatively large increments in Re could be used for $\ell = 1$, but the process became tedious for $\ell = 2,3$. Results for Re = 100, f = 0.1, and $n \leq 5$ are shown in Figure 2. The first eigenvalue on each branch and $k_{3,2}$ are labeled. Note the separation of $k_{3,2}$ and $k_{3,1}$. It increases monotonically with Re; $|k_{3,2} - k_{3,1}|/|\lambda_{3,2} - \lambda_{3,1}|$ is 1.56 for Re = 10 and 4.62 for Re = 100, both for f = 0.1. The ordering of the $k_{\ell,n}$ is determined by the number of zeroes of the eigenfunctions: n zeroes corresponding to $k_{1,n}$ and n - 1 zeroes corresponding to $k_{2,n}$ or $k_{3,n}$. This ordering is consistent with the analytical results obtained in the Stokes limit.

In calculating the flow variables, the $k_{\ell,n}$ must be taken in groups of three: ℓ = 1,2,3 for n = 1, n = 2, etc. Departure from this ordering introduces errors; the error depends mainly on the degree of departure, n and on the method used to calculate α_n.

A more efficient method of estimating $k_{2,n}$ and $k_{3,n}$ for large Re was needed and for this purpose an asymptotic approximation was derived.

3. $Re \to \infty$

An asymptotic solution to (2.3), with m = 1 and K = k, can be found by expanding the disturbance field and wave numbers in the form

$$k = \sqrt{Re}\ \kappa_0 + \kappa_1/\sqrt{Re} + \dots ,$$

$$u = u_0 + \frac{1}{Re} u_1 + \dots ,$$

$$v = v_0 + \frac{1}{Re} v_1 + \dots ,$$

$$w = \frac{1}{\sqrt{Re}} w_0 + \frac{1}{Re^{3/2}} w_1 + \dots ,$$

$$p = \frac{1}{Re} p_0 + \frac{1}{Re^2} p_1 + \dots . \qquad (3.6a,b,c,d,e)$$

The zeroth order approximation to (2.3a,b) then yields

$$\{-\kappa_0^2 - if + i\}\, u_0 + 2v_0 = 0$$

$$\{-\kappa_0^2 - if + i\}\, v_0 - 2u_0 = 0 \qquad (3.7a,b)$$

and the consistency of (3.7a,b) requires that either

$$\kappa_0^2 = -(1 + f)i ,$$

or

$$\kappa_0^2 = (3 - f)i , \qquad (3.8a,b)$$

where Real $\kappa_0 > 0$ is required so that (3.8a) and (3.8b) correspond to branches 2 and 3, respectively. A spectrum is not obtained in this approximation to k.

Corresponding to (3.8a), the zeroth approximation to (2.3c,d) yields

$$p_0 = -2iw_0/\kappa_0$$

$$w_0 = u_0'/\kappa_0. \tag{3.9a,b}$$

where ' = d/dr; u_0 is obtained as follows.

The next order approximation to (2.3a,b) yields a pair of inhomogeneous linear equations for u_1, v_1. The operators in the homogeneous parts of these equations are identical to those in the l.h.s. of (3.7); thus, the inhomogeneous terms must satisfy a solvability condition, which, for κ_0 from (3.8a), reduces to

$$u_0'' + (1/r)\, u_0' + D^2\, u_0 = 0 \tag{3.10}$$

where $D^2 = -2\kappa_0\kappa_1\,(1+f)/(2+f)$ and the required solution is

$$u_0 = J_0(Dr).$$

The κ_0 from (3.8b) leads to

$$u_0'' + (1/r)\, u_0' + (B^2r^2 - 4)\, u_0/r^2 = 0, \tag{3.11}$$

where $B^2 = -2\kappa_0\kappa_1\,(3-f)/(4-f)$ and the required solution is

$$u_0 = J_2(Br). \tag{3.12}$$

The boundary condition $u_0(1) = 0$ determines κ_1 for each branch; their values, corresponding to (3.8a,b,) are given by

$$\kappa_1 = -\,(\sqrt{2}/4)\,(1+i)(2+f)\, j_{0,s}^2 \,/\, (1+f)^{3/2}$$

and

$$\kappa_1 = -(\sqrt{2}/4)(1-i)(4-f)\, j_{2,s}^2 \,/\, (3-f)^{3/2} \tag{3.13a,b}$$

respectively, $s = 1,2,\ldots$. Thus (3.6a), using (3.8a) and (3.13a) or (3.8b) and (3.13b), approximates the eigenvalues on branches 2 and 3, respectively, correct to $O(Re^{-1/2})$. From (3.9b) and the boundary condition $w_0(1) = 0$, a boundary layer of thickness $O(Re^{-1/2})$ must be introduced at $r = 1$ but this does not affect κ_1 given by (3.13). Further asymptotic approximations to the eigenvalues will be reported in a separate publication.

Consider a numerical example: $Re = 1{,}000$, $f = 0.1$ and branch 3. The first term of (3.6a), with (3.8b), gives $\sqrt{1{,}000}\ \kappa_0 = 38.0789\ (1+i)$ while the first two terms, using (3.8b) and (3.13b) with $s = 1$, give an approximation $37.8460 + i\ 38.3117$. Using these as first guesses in the eigenvalue iteration routine, the iteration process diverged for the former but converged for the latter, even if rounded to 2 decimal places. The converged value is $37.8471 + i\ 38.3196$. The iteration process also converged using guesses obtained from the first two terms of (3.6a) and (3.13) with $s = 2$ and 3 but not with $s = 4$. If the third term in (3.6a) is also included, but the boundary layer at $r = 1$ neglected, the iteration process converges for $s \leq 5$.

Although the first term in (3.6a) does not provide a first guess which converges to an eigenvalue, it can be used to obtain a "differential correction" to an eigenvalue. In fact, an extrapolation of the eigenvalue for Re_1, f_1 to Re_2, f_2 can be derived from the first term in (3.6a) which is second order correct in $\Delta Re = Re_2 - Re_1$ and $\Delta f = f_2 - f_1$. For branch 2, the increment in k is

$$\Delta k = \left[\sqrt{1+f_0}\ (1-i)/2\sqrt{2}\ \sqrt{Re_0}\right]\left[\Delta Re + Re_0\ \Delta f/(1+f_0)\right]$$

and for branch 3

$$\Delta k = \left[\sqrt{3-f_0}\ (1+i)/2\ \sqrt{2}\ \sqrt{Re_0}\right]\left[\Delta Re - Re_0\ \Delta f/(3-f_0)\right]$$

where Re_0 and f_0 are the average values of Re_2, Re_1, and f_2, f_1, respectively.

Having calculated just three eigenvalues along each of the branches 2 and 3, the first guess for the next one was obtained using the asymptotic approximation and extrapolation in n. For larger n, the algorithm stated previously was used. Although the asymptotic method for $Re \to \infty$ described here does not give approximations for branch 1, those eigenvalues can be obtained rather easily by extrapolation from $Re = 100$. In Figure 3, the converged eigenvalues, $k_{\ell,n}$, are presented for $Re = 1{,}000$, $f = 0.1$, $\ell = 1,2,3$ and $n \leq 24$.

4. CALCULATION OF α_n.

Reverting to the first notation for the eigenvalues, assume that $\{k_n\}$ are known for $1 \leq n \leq 3M$, where M is a positive integer. Truncating the series in (2.9) at $n = 3M$, the coefficients $\{\alpha_n\}$, $1 \leq n \leq 3M$, were determined by either of two ways. The first is collocation. Let $\{r_j\}$, $1 \leq j \leq M$, be a sequence of points such that

$$0 < r_1 < r_2 \ldots < r_M < 1.$$

Enforcing the boundary conditions (2.7) at the points $r_1, \ldots, r_M$ leads to

$$E_1 (r_j) \equiv \sum_{n=1}^{3M} \alpha_n u_n (r_j) = 0$$

$$E_2 (r_j) \equiv \sum_{n=1}^{3M} \alpha_n v_n (r_j) = 0$$

$$E_3 (r_j) \equiv \sum_{n=1}^{3M} (\alpha_n \cot k_n A) w_n (r_j) + \sigma(r_j) = 0 . \qquad (3.14a,b,c)$$

These 3M linear equations are solved for the coefficients $\alpha_1, \ldots \alpha_{3M}$. The success of the method requires that the flow properties converge in some sense as M increases. Experience has shown, for $Re \leq 1{,}000$, that the required value of M, to achieve a given accuracy, increased monotonically with Re. Numerical examples are given in Section V.

The second is a least squares method. The "normal" equations for α_n are obtained by minimizing the error

$$g(\alpha_n) = \int_0^1 \left\{|E_1(r)|^2 + |E_2(r)|^2 + |E_3(r)|^2\right\} r^e \, dr . \qquad (3.15)$$

Exponents e = 0,1 gave essentially the same results. A measure of the error, E, in α_n is given by

$$E^2 = g/\int_0^1 |\sigma(r)|^2 r^e \, dr. \qquad (3.16)$$

The coefficients of the linear equations for α_n are given in the Appendix.

IV. PRESSURE AND MOMENT COEFFICIENTS

The velocity, pressure and moment exerted by the liquid on the container are quantities of physical interest calculated by the spatial eigenvalue method. The last is of direct use in the application of the theory to the study of projectile stability; e.g., it can be used to calculate yaw growth rate.[4,13] Measurements of pressure have been made mostly on the endwall and the sidewall, an exception being those on the axis of the cylinder by Aldridge.[14] Only the endwall case is considered. The pressure transducer measurements are processed[15] to produce amplitude and phase. This amplitude is compared with calculations in the next section. Comparisons are made using only non-dimensional pressure and moment coefficients. In Reference 16 dimensional quantities are used; these are converted to dimensionless forms for present purposes. Derivations of pressure and moment coefficients are outlined; details can be found in References 4 and 13.

The pressure calculated from the Navier-Stokes equations, p_{NS}, is

$$p_{NS} = 1/2\ r^2 - K_0\ p^* \tag{4.1}$$

in the linear theory. However, since the measurement is made in a reference frame fixed to the cylinder, with coordinates $\tilde{r},\tilde{\theta},\tilde{x}$, the coordinates used in the analysis, r,θ,x, must be transformed to this frame. For example,

$$1/2\ r^2 = 1/2\ \tilde{r}^2 - K_0\ \tilde{r}\ \tilde{x} \cos(ft-\tilde{\theta}) + O(K_0^2)\ . \tag{4.2}$$

The disturbance pressure, Δp, is the pressure not including the contribution from solid body rotation. At points fixed on the surface of the cylinder

$$\Delta p = 1/2\ r^2 - K_0\ p^*\ (\tilde{r},\tilde{\theta},\tilde{x},t) - 1/2\ \tilde{r}^2\ .$$

Using $p^*\ (\tilde{r},\tilde{\theta},\tilde{x},t) = p^*\ (r,\theta,x,t) + O(K_0)$, (1.1) and (4.2),

$$\Delta p = -K_0\ [-\underline{p}_I \sin(ft-\theta) + (\underline{p}_R + rx) \cos(ft-\theta)] \tag{4.3}$$

where sub R and I denote real and imaginary parts of $\underline{p}$, respectively, and the $\tilde{r}\tilde{x}$ factor in (4.2) can be replaced by rx without changing the order of approximation; (2.6d) relates $\underline{p}_R$, $\underline{p}_I$ to p_R, p_I and the latter are obtained from (2.9d). Note that $\underline{p}_R + rx = p_R + f^2rx$ and $\underline{p}_I = p_I$. The pressure coefficient, C_p, is defined as the amplitude of $\Delta p/K_0$, i.e.,

$$C_p = [(\underline{p}_R + rx)^2 + \underline{p}_I^{\,2}]^{1/2}. \tag{4.4}$$

Certain limiting forms of C_p can be derived. Firstly, consider $f \to 0$. From (2.7c), the boundary condition is

$$w = f\omega(r) \quad , \qquad x = \pm A$$

so that the α_n from (3.14) and (u,v,w,p) in (2.9) are $O(f)$. Therefore,

$$(u,v,w,p) = f\,(u^o,v^o,w^o,p^o) + O(f^2)$$

where (u^o, v^o, w^o, p^o) expand as in (2.9). The eigenvalues are evaluated for $f = 0$ and the endwall boundary condition is

$$w^o = \omega\,(r) \quad , \qquad x = \pm A \ ,$$

which leads to

$$C_p = |f| \left\{ \left| \sum_{1}^{3M} \alpha_n\, p_n^o \right|^2 \right\}^{1/2} + O(f^2) \ . \tag{4.5}$$

For Re = 8.8, A = 3.148 and r = 0.667, (4.5) gives

$$C_p = .82\ |f| + O(f^2) \ .$$

For large values of f, the endwall boundary condition becomes

$$w = -2ifr + O\left(e^{-|f|^{1/2}}\right), \qquad\qquad x = \pm A$$

for $r \gg |f|^{-1/2}$; this is obtained by using the asymptotic expansions for $J_1(\lambda r)$ and $J_1(\lambda)$ in (2.7c). Thus, the flow has a boundary layer structure of thickness $O\,(|f|^{-1/2})$ at $r = 0$ which implies that ε (see Section III) must be chosen such that $\varepsilon \ll |f|^{-1/2}$. From (3.14c) and (2.9d) $p \sim |f|$ and a first approximation, neglecting the $O\,(|f|^{-1/2})$ boundary layer, gives

$$C_p = f^2\, r\, A + O\,(|f|) \tag{4.6}$$

on the endwall.

If $f = 1$, the perturbation is zero which is clear from (2.6), (2.7), and (2.8). Therefore, (4.4) gives

$$C_p = rx \quad , \quad f = 1 \, , \tag{4.7}$$

a linear variation on the endwall and sidewall. Since (4.7) is exact, it can be used in error analyses of the numerical results.

For $r \ll 1$, it can be shown that, on the endwall, for all Re and f

$$C_p = O(r). \tag{4.8}$$

The moment exerted by the liquid on the container can be calculated from the rate of change of angular momentum[3,6] or from the integration over the cylinder surface of the pressure and shear forces.[4,13,16,17] The latter is outlined. The three components of the moment are evaluated in an aeroballistic coordinate system. The axial or roll component is zero to $O(K_0)$; the transverse components are $O(K_0)$ and, to that order, are the same in the aeroballistic and inertial frames. The transverse components can be separated into the overturning or side moment and the in-plane moment which acts to change the coning rate.[17] The side moment is important for projectile stability, as shown by Murphy,[17] and is the only component considered. The following definitions[17] are used: *nondimensional side moment coefficient* $\equiv$ C_{LSM} = side moment$/2\pi\rho a^4 c (\bar{\tau} + \Omega)^2 f K_0$; C_{LSM} is expressed as the sum of the four contributions: the pressure on the sidewall, pressure on the *endwalls, shear force on the sidewall and shear force on the endwalls.* These are given by

$$(fA)^{-1} \int_0^A x \, \underline{p}_I \, (1,x) \, dx$$

$$-(fA)^{-1} \int_0^1 \underline{p}_I \, (r,A) \, r^2 \, dr$$

$$-(fARe)^{-1} \int_0^A \left[\partial \, (x\underline{v}_R - \underline{w}_I)/\partial r \, \Big|_{r=1} + 1 - f \right] dx$$

$$-(f \, Re)^{-1} \, \mathrm{Real} \left[1 - f + \int_0^1 \partial \, (\underline{v} - i\underline{u})/\partial x \, \Big|_{x=A} r \, dr \right] \tag{4.9a,b,c,d}$$

respectively.* For the reasons given in deriving (4.7) $C_{LSM} = 0$ for $f = 1$. The derivative in (4.9d) will introduce a factor k_n in the series used to calculate (4.9d) which, it was conjectured, would adversely affect convergence. By integrating (2.8a,b) over x and r, an alternative form was derived which did not have this factor. It was found, numerically, that the two forms agree to 2% or less for $|k_n| \sim 100$.

If the pressure and moment coefficients are defined using the spin, Ω, and non-dimensional coning frequency, τ', relative to S', and denoted by C_p' and C_{LSM}', they are related to C_p and C_{LSM} by $C_p = C_p' (1 - f \cos K_0)^2$ and $C_{LSM} = C_{LSM}' (1 - f \cos K_0)$.

V. RESULTS

A sampling of results obtained by the spatial eigenvalue method is given. Some of these are used to discuss the numerical process but most of the results presented either have intrinsic interest or are used to compare with finite difference calculations or experiment. A standard set of the basic parameters was chosen to facilitate comparison of several of the figures; these are Re = 10, f = 0.1, A = 3.0. Since the original motivation for this work was the calculation of C_p and C_{LSM} for "small" Re, this range is emphasized here. For "large" Re, the theories of References 4, and 13 are available.

Instead of an analysis of the numerical processes used in the spatial eigenvalue method, a number of empirical studies were made, and some conclusions based on these are presented. Recall that two methods were used for determining the eigenvalues, viz., orthonormalization[10,11] and finite difference,[12] and that two methods were used to determine the coefficients, α_n, viz., collocation and least squares. As expected, results were not very sensitive to the choice of method for computing $k_{\ell,n}$. Extensive calculations were made with a program combining orthonormalization with least squares and another combining the finite difference technique with collocation; these are denoted by LS and COL, respectively.

Of the physical parameters, the calculation is more sensitive to Re and f than A; recall that the $k_{\ell,n}$ are independent of A. Of the numerical parameters, obviously the number of eigenvalues, N = 3M, is most important; in COL the number of collocation points is M. In all calculations using collocation, the collocation points were equally spaced (exactly or to within ±1 of the point number). The number of points required in the numerical integration of the differential equations for the eigenfunctions is directly related to N. A number of points equal to 7M was found to be adequate although a larger number was usually employed; recall that the largest number of zeroes of the eigenfunctions is M. There are several other numerical parameters having to do with the number of terms in series, convergence of iteration processes, etc, which will not be discussed.

*In (4.9) the complete expressions for shear stress are used whereas approximations for large Re are introduced in Reference 13.

The first illustration is for the calculation of C_{LSM} by LS and COL for the case Re = 21.5, f = .0621, A = 1.042 and $3 \leq N \leq 42$, shown in Figure 4; there is a break in the ordinate scale to accommodate the COL point for N = 9. The LS results are less sensitive to decreasing N than the COL results. The LS value for N = 6 is within 1.7% of the result for large N and required only 6 seconds of CPU time on the VAX 8600. The LS and COL results are essentially the same for $N \geq 12$. A comparison with an experimental result is shown later for the same Re, f, and A used here.

The calculated values of C_p (.667) vs N, using LS and COL, are shown in Figures 5 and 6 for Re = 100 and 1,000, respectively, and f = 0.1, A = 3. In Figure 5 the differences in C_p for $N \geq 36$ are negligible. At N = 12, the LS value is 0.13% below and the COL value is .41% below the result for N = 72. In Figure 6 the approach to a limiting value for large N is not as clear. The LS and COL results differ by 1% at most for $N \geq 48$. The limiting value is approximately C_p (.667) = .205. At N = 12 the COL value is 2.4% below the limiting value, and the LS value, offscale, is 7.8% below the limiting value.

In all the cases discussed hereafter, N was chosen large enough to give limiting values of C_p and C_{LSM} in the sense used above, and the values obtained using LS and COL agreed to at least three significant figures with the exception of the C_{LSM} vs A results for Re = 1000. When quoting results from finite difference methods, for comparisons, K_0 must be specified; results from the linear theory used here are independent of K_0, of course.

The variation of C_p with r, on the endwall, is shown in Figure 7 for Re = 1.0, f = 0.1, and A = 3.0. In addition, results[7] from Strikwerda's method are presented for $K_0 = 2°$. The former is essentially linear with r for approximately $0 \leq r \leq 0.2$ but the latter is not. From (4.8), $C_p = O(r)$. This comparison and some others indicate a loss in accuracy of Strikwerda's method for $Re \leq 1$.

In Figure 8, the spatial eigenvalue calculation of C_p on the endwall vs f is presented for Re = 10 and A = 3.0 at r = 0.5 and 1.0. Recall that $C_p = O(|f|)$ for $f \to 0$, from (4.5), but the dependence is not linear over $0.1 \leq f \leq 1.0$. Values of C_p from the asymptotic approximation (4.6) are also given. At f = 0.8 and r = 1, the estimate (4.6) is 8% lower than the calculation; at f = 1.1 (not shown) and r = 1, it is 3% higher.

The variation of C_p on the endwall, x = A, at r = .667, over the range $1 \leq Re \leq 1000$ and for f = 0.1, A = 3 is shown in Figure 9. Over that range, C_p varies by a factor of 2.3.

The variation of C_p at $x = A$, $r = .667$, over the range $0.5 \leq A \leq 15$ and for Re = 10, f = 0.1 is shown in Figure 10. In projectile application usually $1 \leq A \leq 5$; over that range C_p increases by a factor of 1.3.

A comparison of calculated pressure coefficient vs f with some experimental measurements of Hepner, Kendall, Davis, and Tenly[15] is shown in Figure 11 for Re = 3.1 and A = 3.148. The pressure transducer was located at r = 0.667 and the coning angle was $K_o = 2°$. The radius of the cylinder was 3.18 cm; the fluid had a density of 0.969 gm/cm^3 and a kinematic viscosity of 60,000 cs. According to Nusca and D'Amico[18] the measured C_p and f are in the inertial reference frame, S. The data include estimates of errors in C_p, as presented by Hepner et al.[15] For almost all points, the calculated C_p is less than the measured C_p; for the larger f it is outside the error bar. The reason for the bias in this comparison is not known.

The remainder of this section is devoted to presentation of results of calculating C_{LSM} and some comparisons. There are more publications that report calculation of C_{LSM} than C_p, starting with the first application of a finite difference method to this problem by Vaughn, Oberkampf, and Wolfe.[16] However, no attempt will be made to be complete in the comparisons, but rather representative.

For $0 < Re \leq 1.0$, f = 0.1 and A = 3.0, the variation of C_{LSM} with Re is linear according to results in Figure 12; the maximum discrepancy in C_{LSM} is 0.3×10^{-4} at Re = 1.0.

In Figure 13 C_{LSM} vs Re is shown for f = 0.1 and A = 3.0. Over the range $1 \leq Re \leq 100$, there is a barely discernable maximum at Re = 50, approximately. For Re > 100, C_{LSM} decreases.

The variation of C_{LSM} with f is given in Figure 14 over the range of $0 \leq f \leq 1.1$ for the spatial eigenvalue calculations and $.05 \leq f \leq 0.9$ for the Strikwerda results, $K_o = 2°$, both for Re = 10.0 and A = 3.0. In practice f < 1.0 but note that $C_{LSM} < 0$ for f = 1.1. The two sets of results are essentially the same, which tends to support the validity of each. The maximum difference is .0025 at f = .6. The existence of a maximum in this curve is of some interest. When the first measurements of C_{LSM}, from yaw growth rate, were made at "small" Re, a linear variation of C_{LSM} with f was found, but only over the range $0 < f < 0.15$. It was speculated that for "small" Re a Stewartson resonance[1] does not occur. Figure 14 shows that resonance does occur at Re = 10, albeit, highly damped. Of course, Stewartson's theory was formulated for an inviscid fluid and its extensions apply to "large" Re so that quantitative results from these could not be expected to apply at Re = 10.

A comparison of calculated side moment coefficient vs f with some experimental measurements of D'Amico[19] is shown in Figure 15 for Re = 21.5 and A = 1.042. The experimental results for $K_0 \approx 2°$ were deduced from yaw growth rate measurements on a gyroscope; according to Nusca and D'Amico,[18] the C_{LSM} and f are in S. The calculations show that C_{LSM} is linear for $0 \leq f \leq .04$, approximately. The experimental results for the two larger values of f lie on the calculated C_{LSM} vs f line, essentially. The reason for the discrepancy at f = 0.045 is not known although it is pointed out in Reference 19 that, as C_{LSM} decreases, the error in its measurement increases; no error bounds were presented.

A similar comparison is shown in Figure 16 for Re = 133 and A = 1.486. The experimental data[19] is for $K_0 < 5°$; C_{LSM} was deduced from yaw growth rate data. The calculations show that C_{LSM} is linear for $0 \leq f \leq .03$, approximately. The gyroscope data are uniformly below the calculated results; no error bounds were presented. If extrapolated, the trend of the data implies $C_{LSM} \approx 0$ at f = 0.03, approximately, and negative values for f < 0.03. In all cases computed thus far, C_{LSM} is positive for 0 < f < 1.

Next, C_{LSM} vs A is presented in Figure 17 for Re = 10 and f = 0.1. The variation is rapid in the neighborhood of A = 1 but for $3 \leq A \leq 15$, C_{LSM} increases by only 3%. The results in Figure 17 can be used to assess the assumption of infinite aspect ratio in Herbert's theory.[3] For Re = 10 and f = 0.1, his theory gives C_{LSM} = -0.114 which is quite different from results in Figure 17. Since the contributions of Eqs. (4.9a,b,d,) to C_{LSM} are identically zero according to his theory, another point of view is to compare his result with that obtained from only Eq. (4.9c), using the present results; this is -0.184 for A = 15, Re = 10, and f = 0.1. The presence of the endwalls appears to have a significant effect on the contribution to C_{LSM} of the shear force on the sidewall, even for A = 15.

The variation of C_{LSM} with A is quite different for Re = 1000, f = 0.1 as shown in Figure 18. The calculations using LS and COL both produce resonant response curves but the computed values of C_{LSM} differ more than in the comparisons shown in Figures 4, 5, and 6; near the maximum of C_{LSM}, which occurs at A = 1.12 for COL, they differ by 11%. For Re = 1000, the limiting values of C_{LSM} are not determined as accurately as for smaller Re or for C_p; the numerical process responsible for that is not understood. The only guidance as to which of the calculations is the more accurate is provided by the third set of results in Figure 18, labeled asymptotic, computed using the theory of References 4 and 13 which is asymptotic for $Re \to \infty$. The comparisons of results from that theory with measurements of yaw growth rate given in Reference 13 indicate that in the neighborhood of Re = 1000, f = 0.1 and A = 1 this asymptotic theory is reliable, but the conclusion is not definitive. The differences between the COL and asymptotic results are less than the corresponding LS differences but the situation is too tentative to draw conclusions concerning the accuracy of either method. Both LS and COL results should tend, for increasing Re, to those of the asymptotic theory for decreasing Re. Qualitatively, this tendency is illustrated in Figure 18 for Re = 1000.

Despite the difference just discussed, the existence of the resonant response, wherein the cavity, i.e., liquid-filled cylinder, is tuned by aspect ratio, is shown in Figure 18. A resonant response is also obtained in the C_p vs A results; the maximum C_p is at A = 1.12. Usually, resonant response tuned by f is investigated in this problem; but the possibility of tuning by A is not surprising considering oscillatory systems, in general. For fixed A = 1.12 and varying f calculations by the asymptotic method give, in addition to the maximum of C_{LSM} at f = 0.1, a secondary peak at f = 0.5.

An attempt was made to compare the moment coefficients calculated by this linear theory to those obtained from the large scale numerical metnods in which linearity in K_0 is not assumed. In addition to the finite difference method of Reference 6, a finite element method was recently applied to this problem by Rosenblat[20] from which a limited number of results is available. Results for moment coefficient, with $K_0 = 20°$, are presented in Table 1 from these methods and the spatial eigenvalue method. The test was frustrated because the results using the methods of References 6 and 20 differ significantly, as seen in Table 1. Therefore, the effects of departure from linearity at $K_0 = 20°$ cannot be judged. In Table 1 Reynolds number, frequency and moment coefficient are given in the aeroballistic reference frame, S', used in References 6 and 20, and denoted by Re', τ', and C_{LSM}'; the transformations relating these to the corresponding quantities in S were given earlier. The comparisons are made in S' because fewer calculations were required.

TABLE 1. Comparison of C_{LSM}' by the Spatial Eigenvalue, Finite Difference and Finite Element Methods; $\tau' = 0.1670$, A = 4.29, $K_0 = 20°$.

	C_{LSM}'		
Re'	Ref. 6,7	Reference 20	Spatial E.V.
5.90	0.03172	0.03082	0.03104
11.42	0.4732	0.04378	0.04785

The differences between the spatial eigenvalue results and those of Reference 20 are 0.7% and 10% for Re' = 5.90 and 11.42, respectively. Between the spatial eigenvalue results and those from Reference 7, the corresponding differences are 2.2% and 1.1% which are no greater than the differences between these methods for $K_0 = 2°$. Although a wider range of parameters must be investigated to arrive at a definitive conclusion, it appears that the nonlinear effect is small up to $K_0 = 20°$.

VI. DISCUSSION

It has been demonstrated that the linearized Navier-Stokes equations with boundary conditions appropriate to a spinning, coning cylinder can be solved by eigenfunction expansions over a wide range of the governing nondimensional parameters: Re, f, and A. By expanding the complete solution in powers of a small parameter related to coning angle, the nonlinear problem can also be solved by eigenfunction expansions. The limitations of the linear theory could be judged by comparison with finite difference or finite element methods, but this is not yet feasible.

The method presented here is in the class of spectral methods. Another spectral method using Chebyshev polynominals has been developed by Herbert;[21] results from his method are not yet available for comparison. Many different solutions for the fluid motion in a spinning, coning cylinder are now available. Judgments on the relative merits of these should be made. To a limited extent, this was done in this report.

Certain deficiencies in the spatial eigenvalue method, for Re $\geq$ 500, were noted. Ideas for removing these are being exploited.

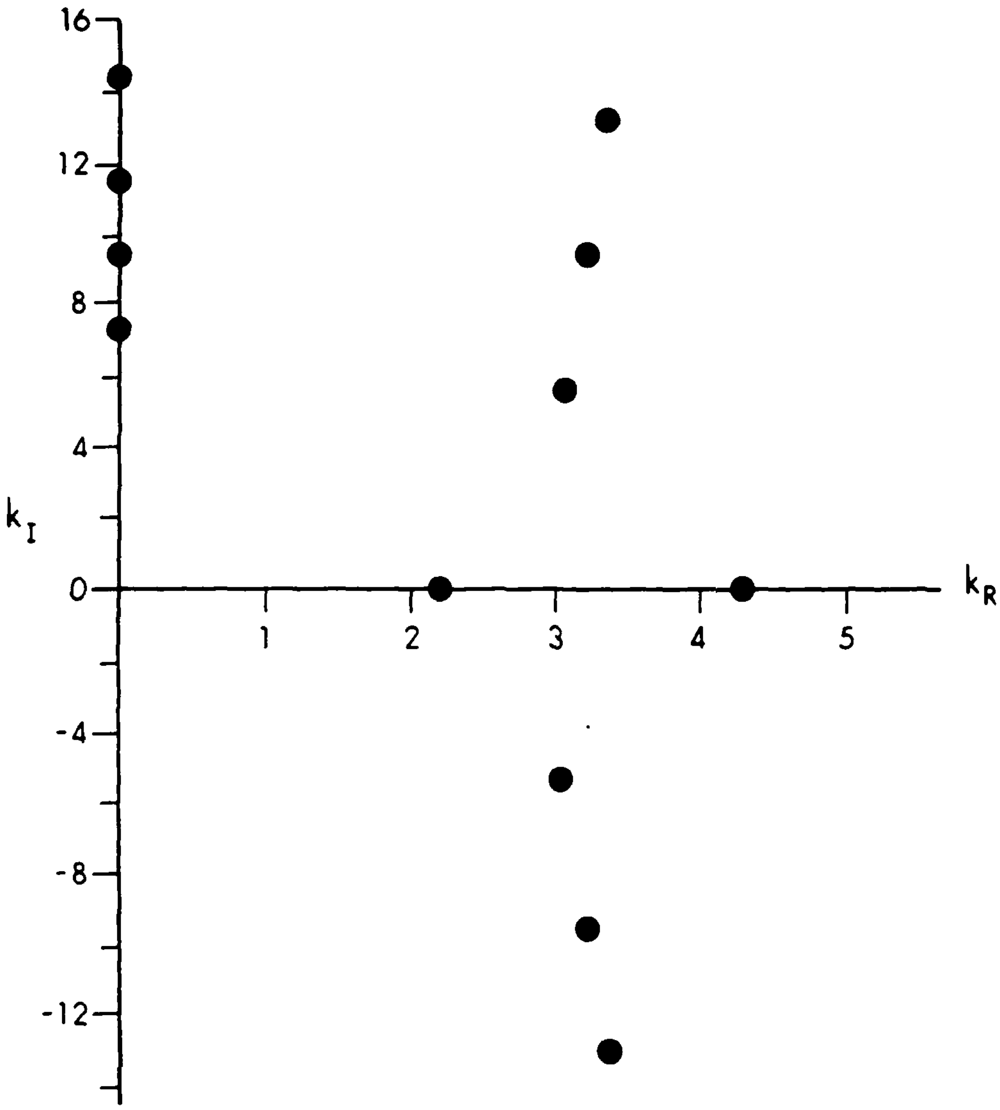

Figure 1. The eigenvalue distribution for the Taylor vortex problem at a small supercritical Reynolds number.

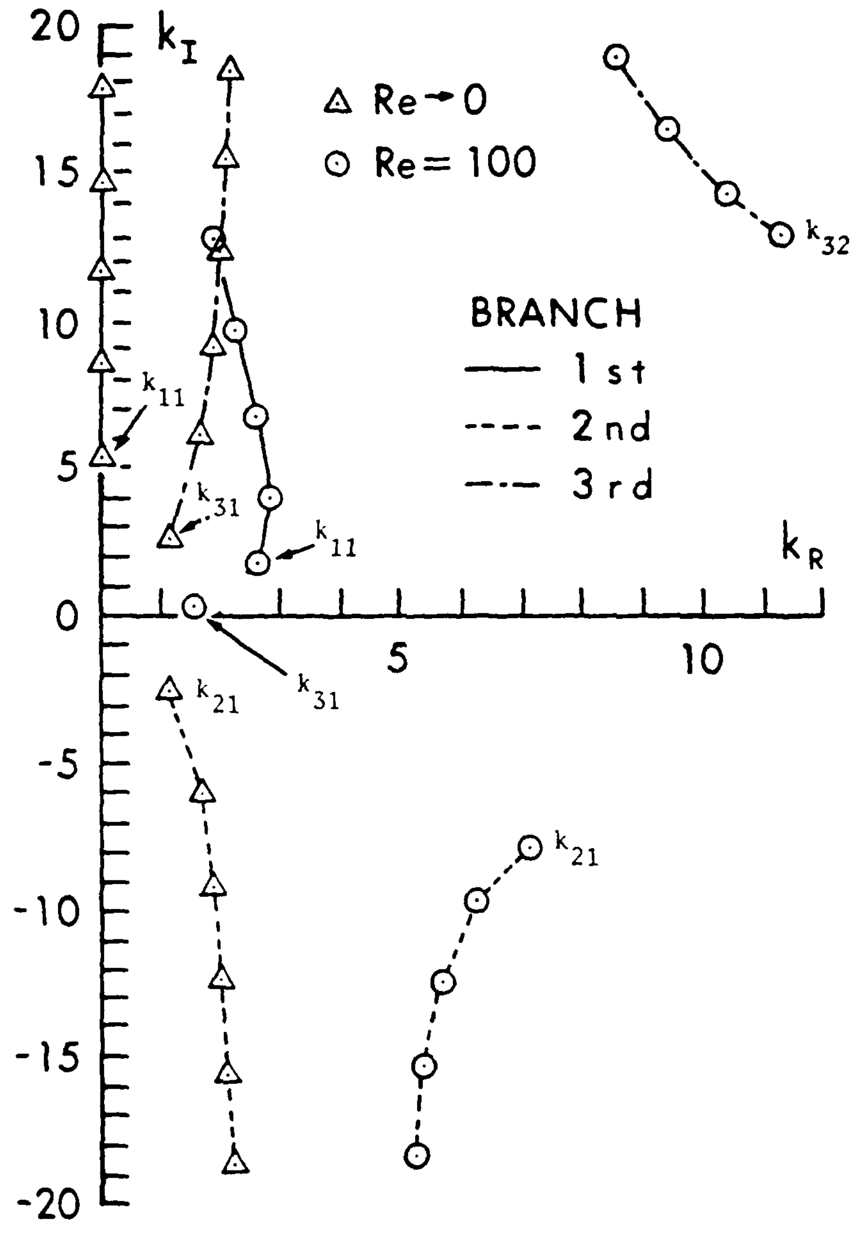

Figure 2. The first 15 eigenvalues for the Stokes limit and for Re = 100, f = 0.1.

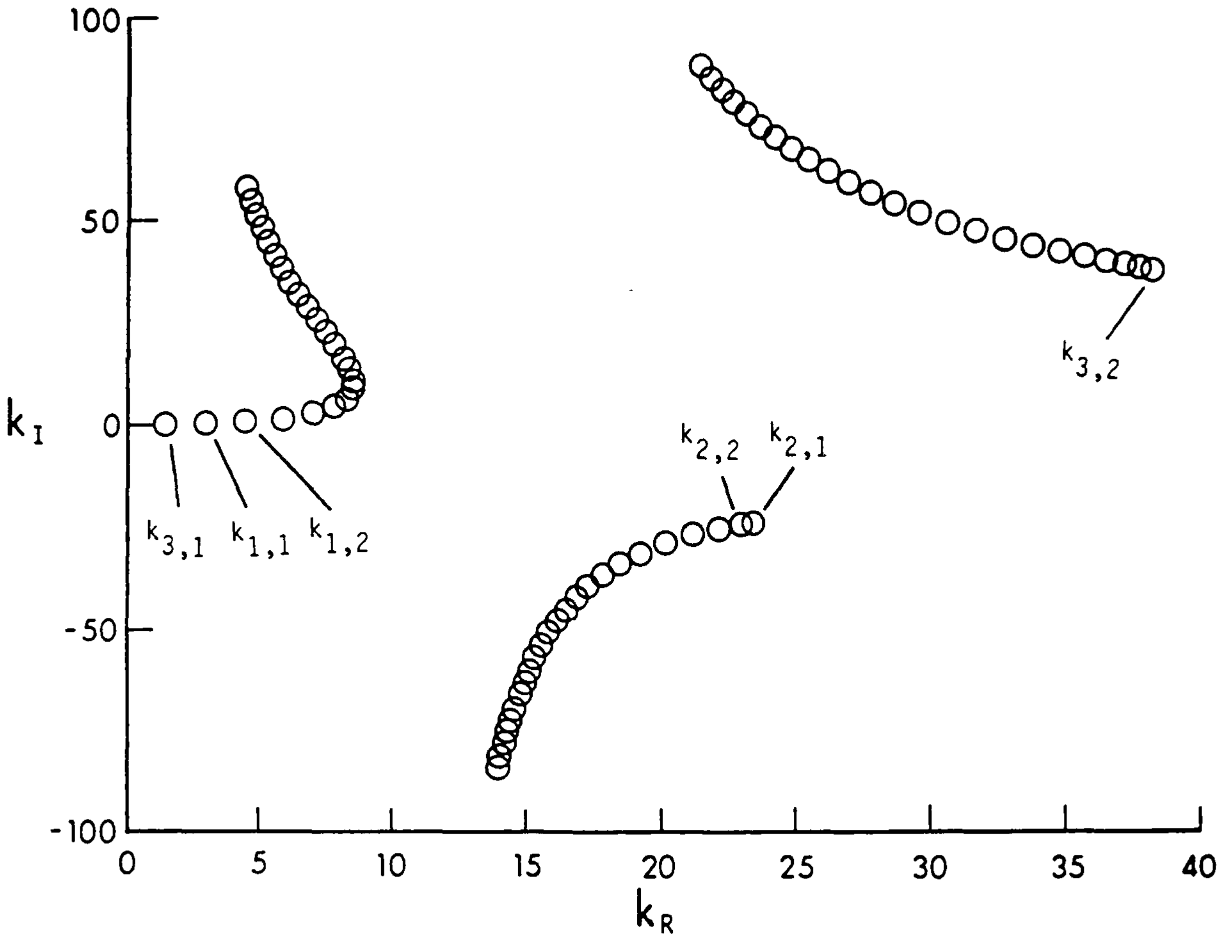

Figure 3. The first 72 eigenvalues for Re = 1000, f = 0.1.

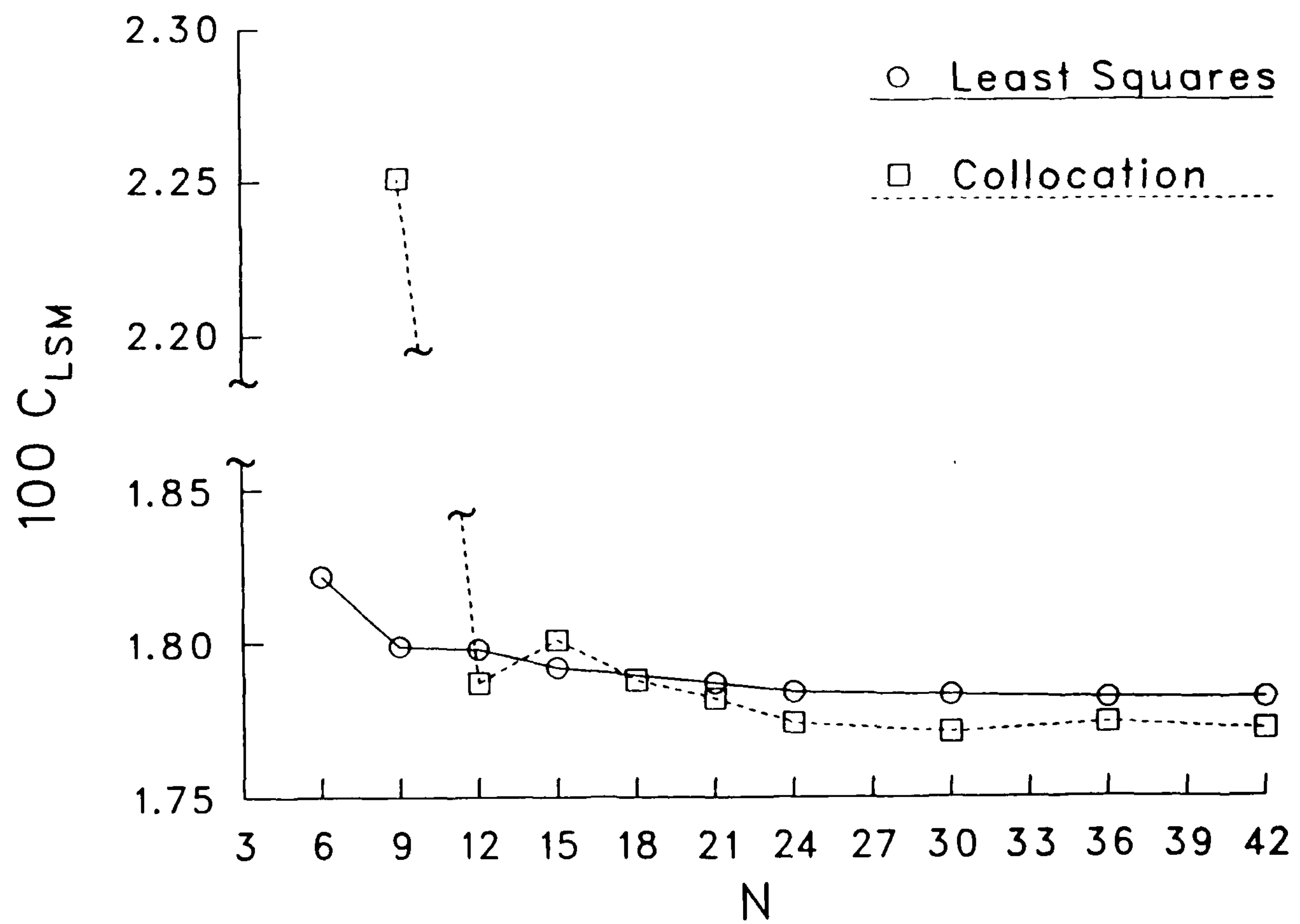

Figure 4. Moment coefficient vs number of eigenvalues for Re = 21.5, f = 0.0621, and A = 1.042 calculated by LS and COL (note break in ordinate scale.)

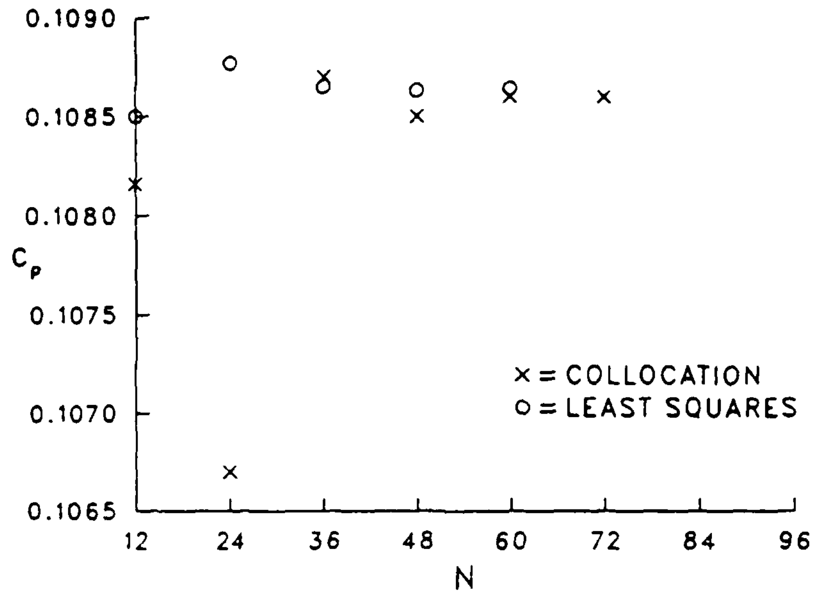

Figure 5. Pressure coefficient at r = 0.667 vs number of eigenvalues for Re = 100, f = 0.1, and A = 3.0 calculated by LS and COL.

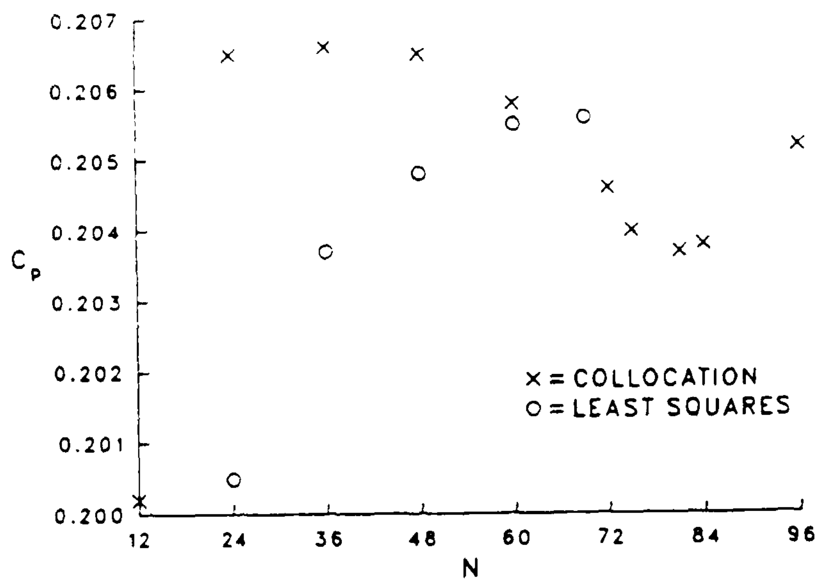

Figure 6. Pressure coefficient at r = 0.667 vs number of eigenvalues for Re = 1000, f = 0.1, and A = 3.0 calculated by LS and COL.

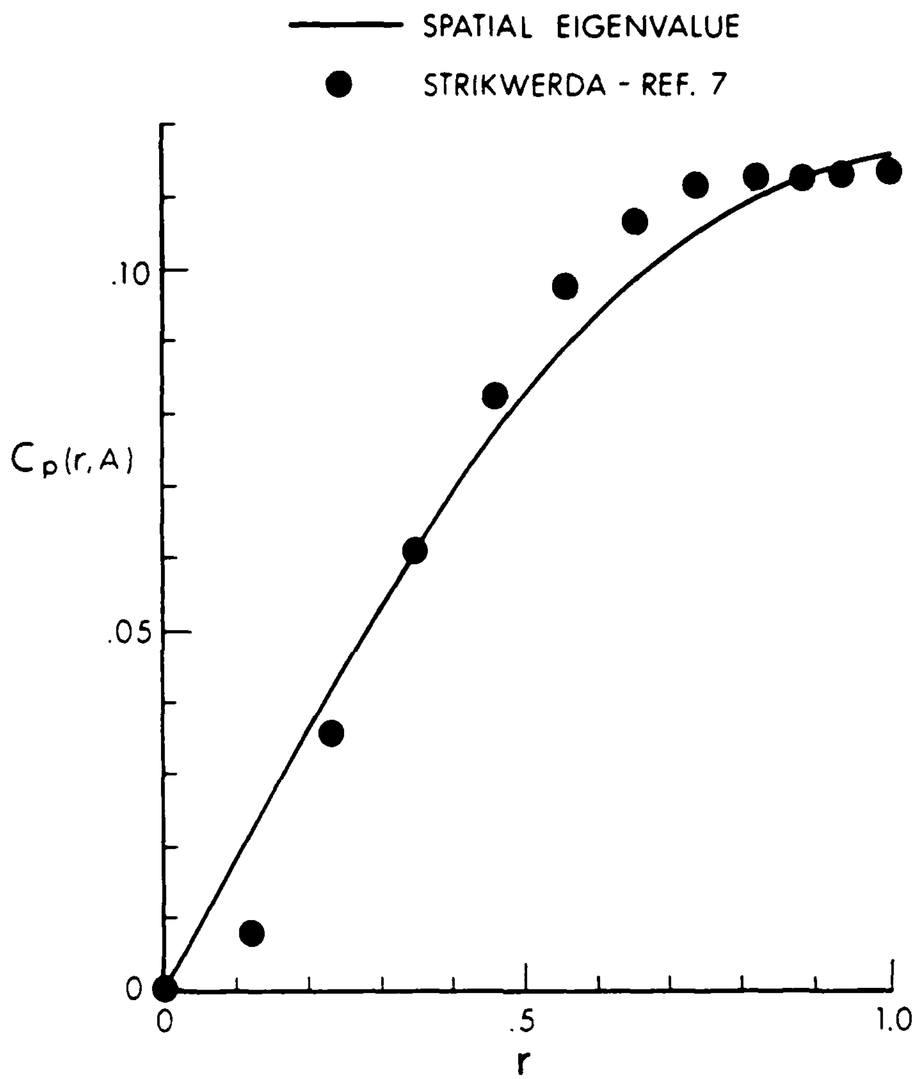

Figure 7. Comparison of $C_p(r,A)$ from the Strikwerda, $K_o = 2°$, and spatial eigenvalue methods for Re = 1.0, f = 0.1, and A = 3.0.

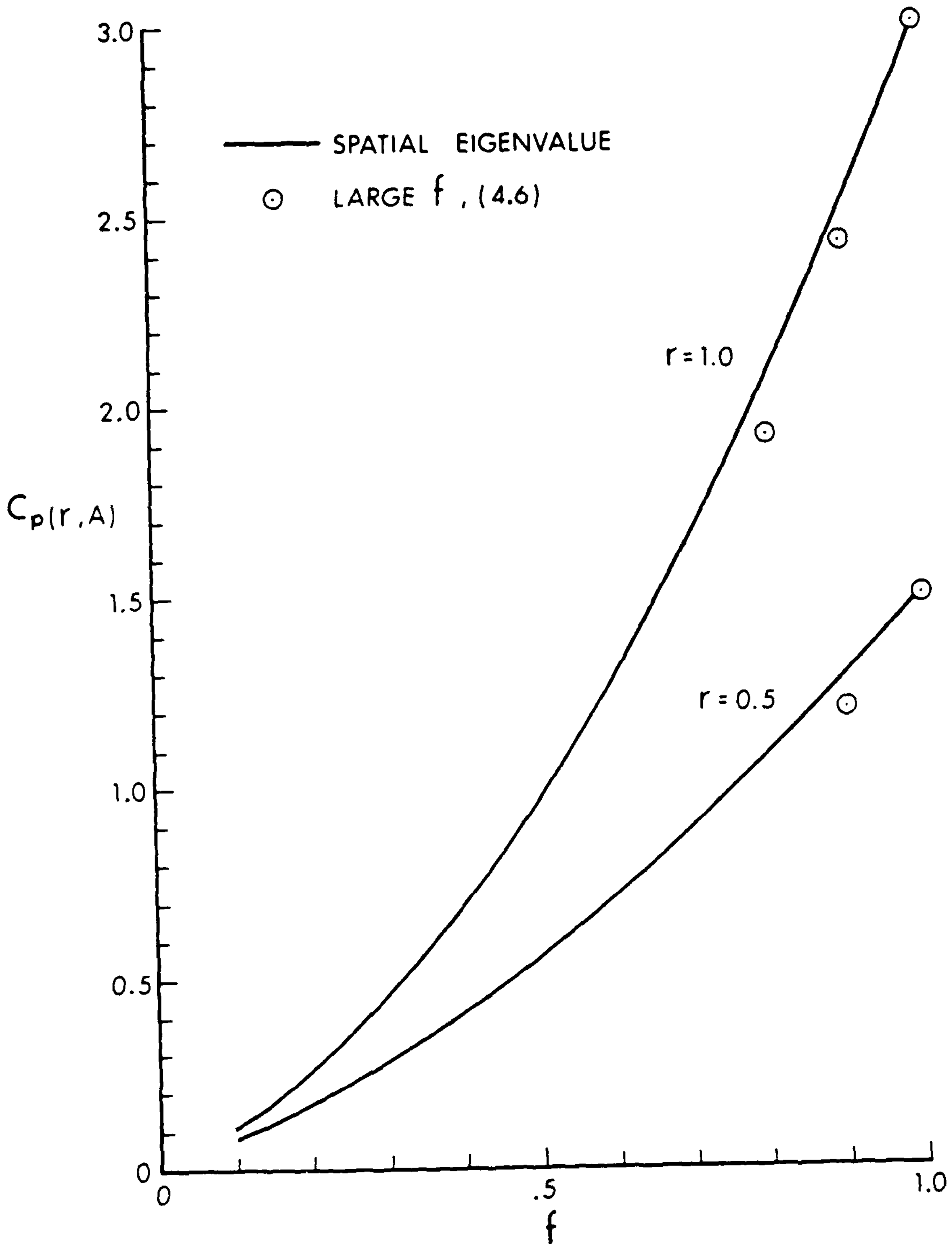

Figure 8. Pressure coefficient, at x = A and two values of r, vs f for Re = 10 and A = 3.0, according to the spatial eigenvalue method and the asymptotic approximation (4.6).

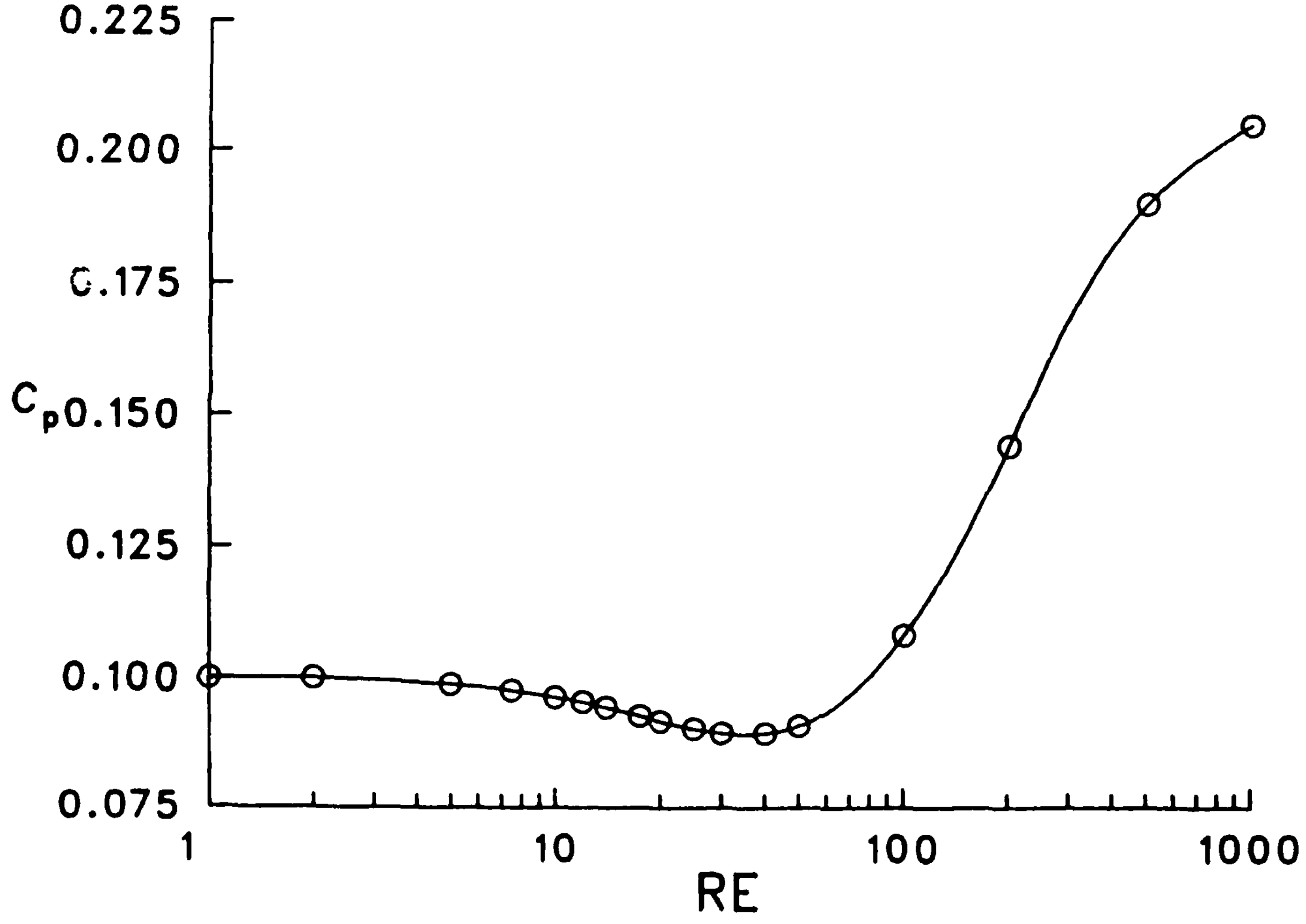

Figure 9. Pressure coefficient at x = A and r = 0.667 vs Re for f = 0.1 and A = 3.0.

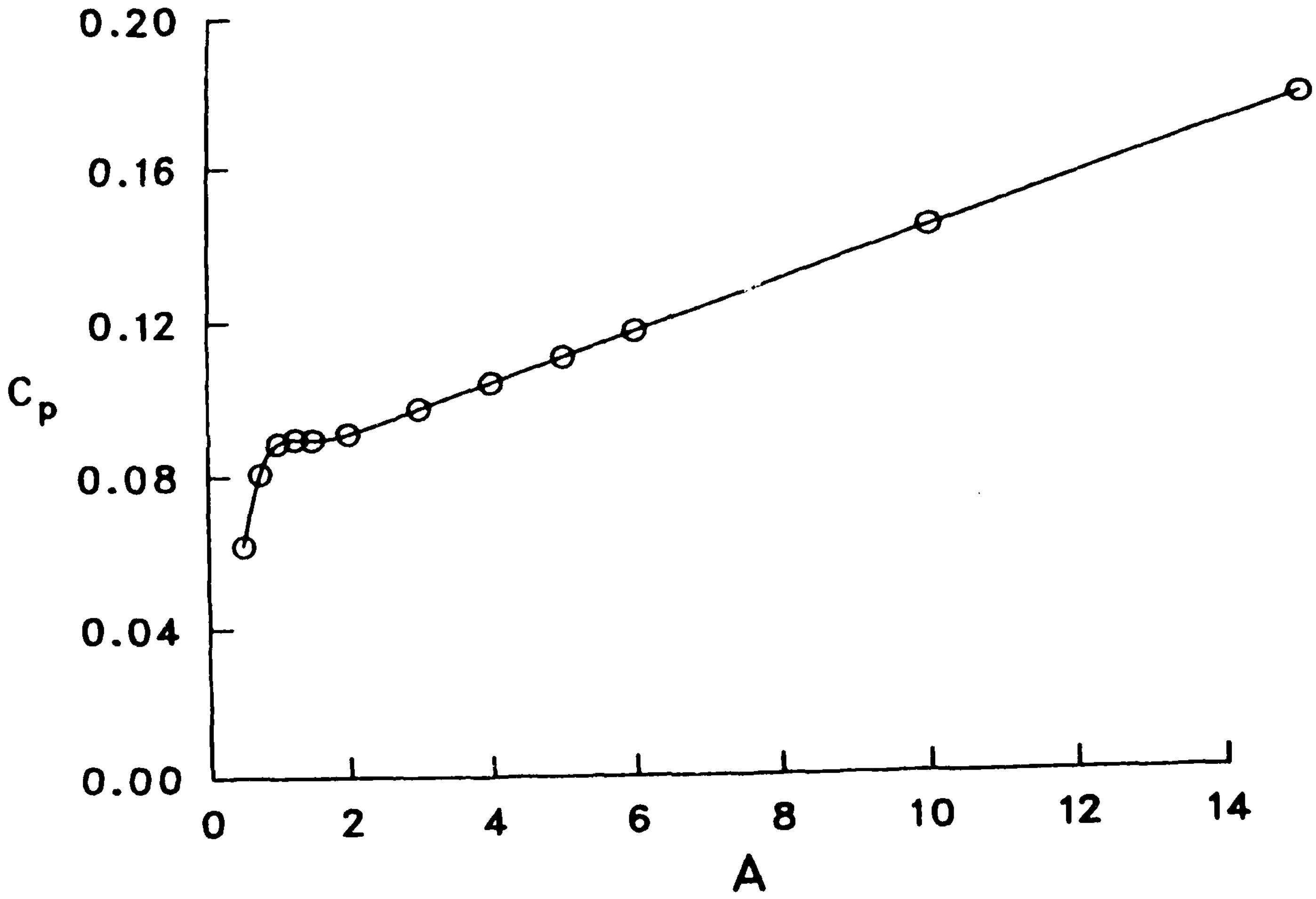

Figure 10. Pressure coefficient at x = A and r = 0.667 vs A for Re = 10 and f = 0.1.

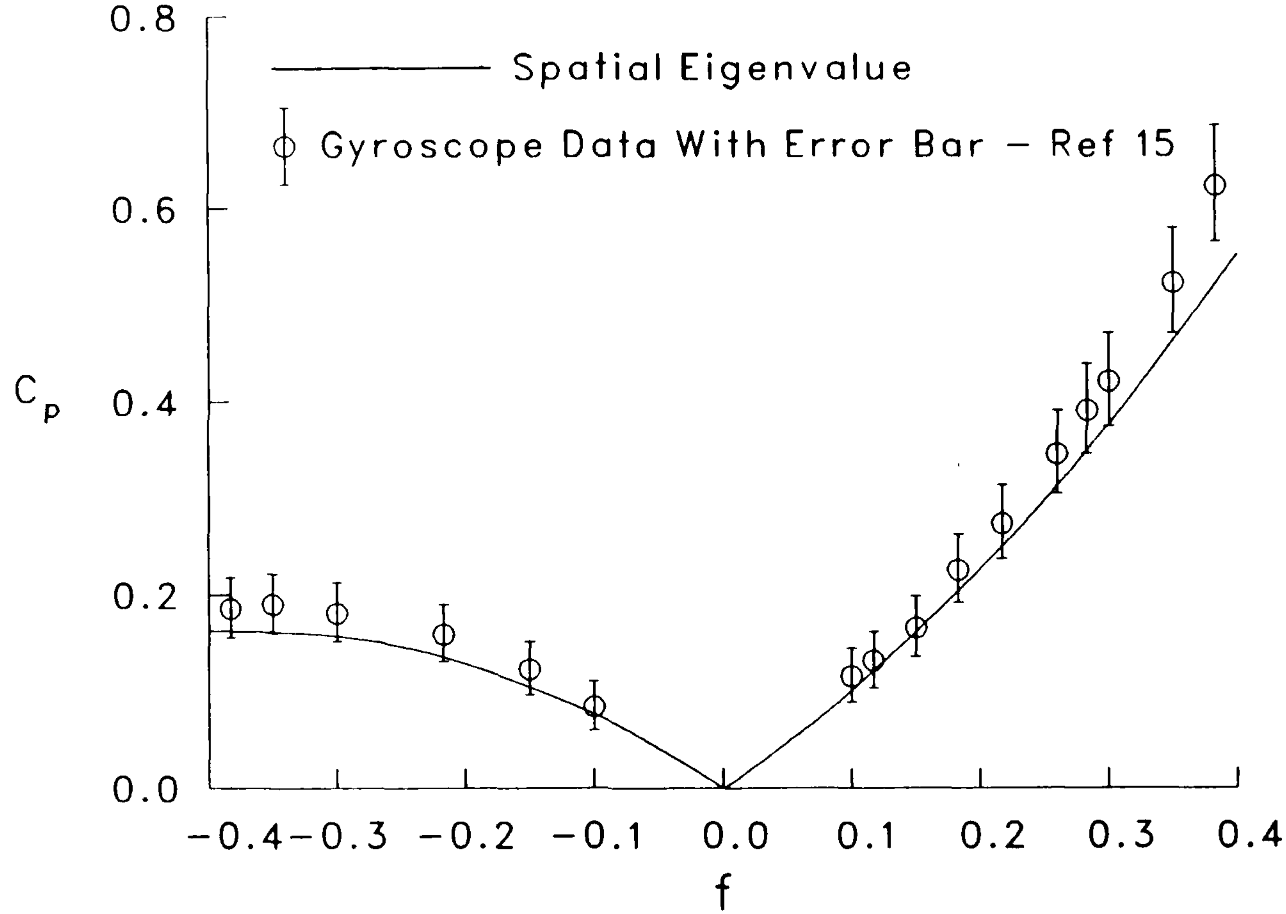

Figure 11. Calculated pressure coefficient vs f compared with experimental measurements from Reference 15 for Re = 3.1, Λ = 3.148, and r = 0.667; for the experiment K_o = 2°. Estimates of errors in the measurements, from Reference 15, are included.

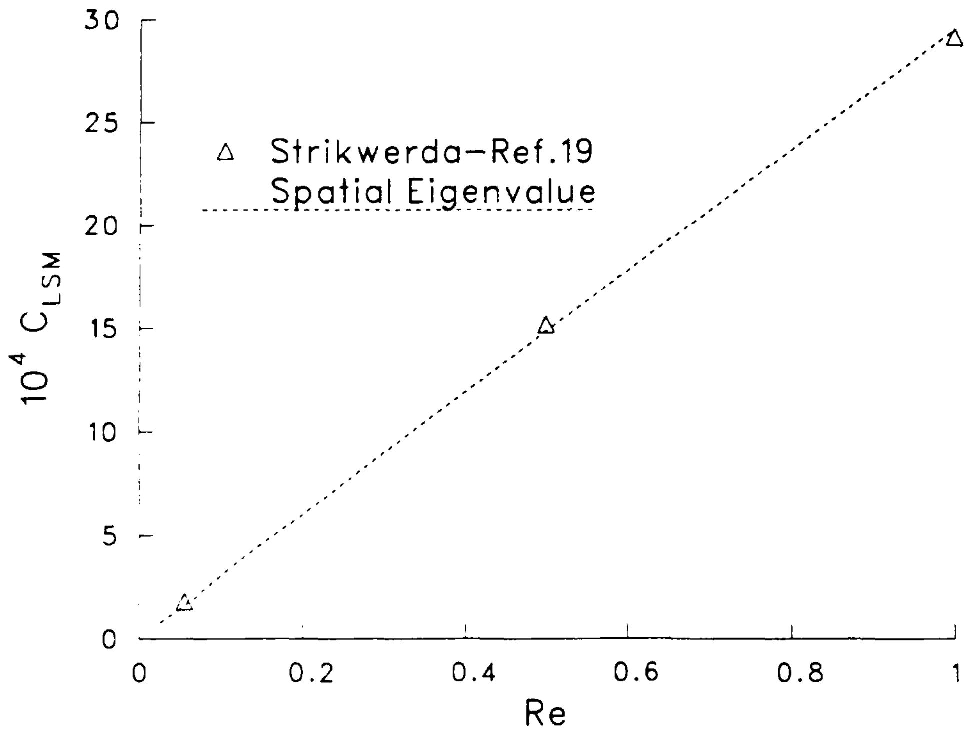

Figure 12. Moment coefficient vs Re for f = 0.1, A = 3.0 according to the spatial eigenvalue method and Strikwerda's method, $K_0 = 2°$, $0 < Re \leq 1.0$.

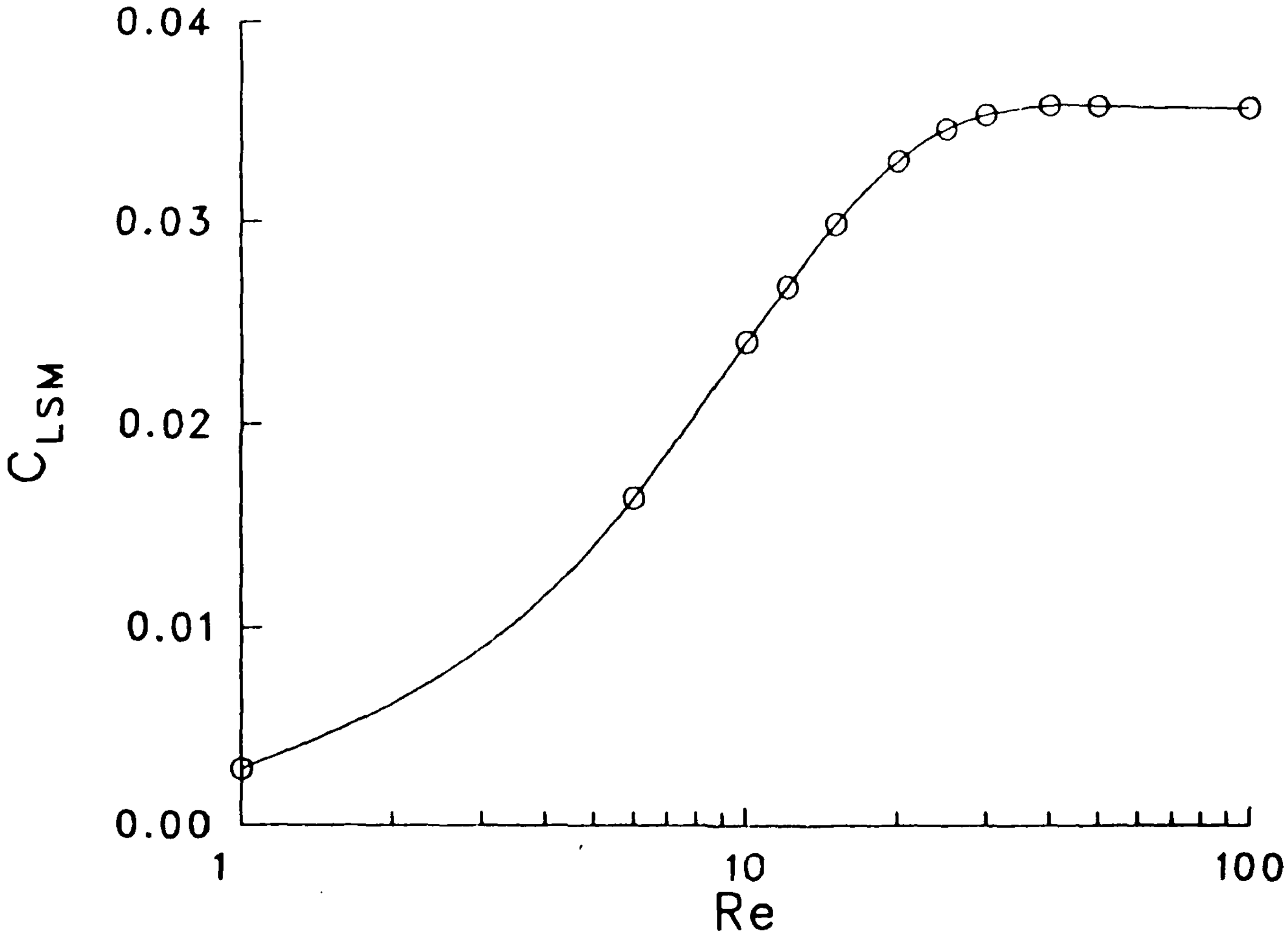

Figure 13. Moment coefficient vs Re for f = 0.1, A = 3.0, 1 ≤ Re ≤ 100.

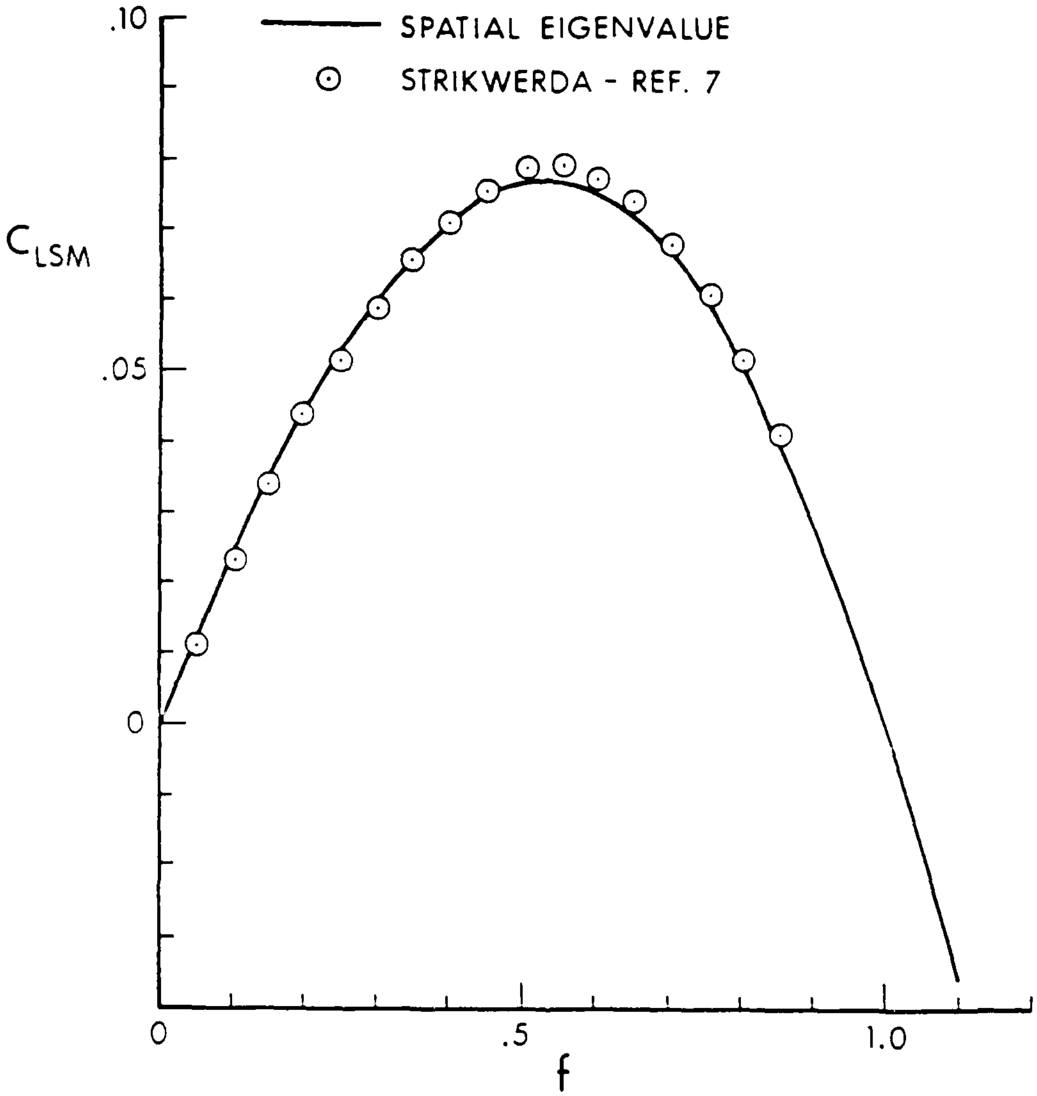

Figure 14. Moment coefficient vs f for Re = 10, A = 3.0; $0 \leq f \leq 1.1$ for the spatial eigenvalue results and $.05 \leq f \leq 0.9$ and $K_0 = 2°$ for the Strikwerda results.

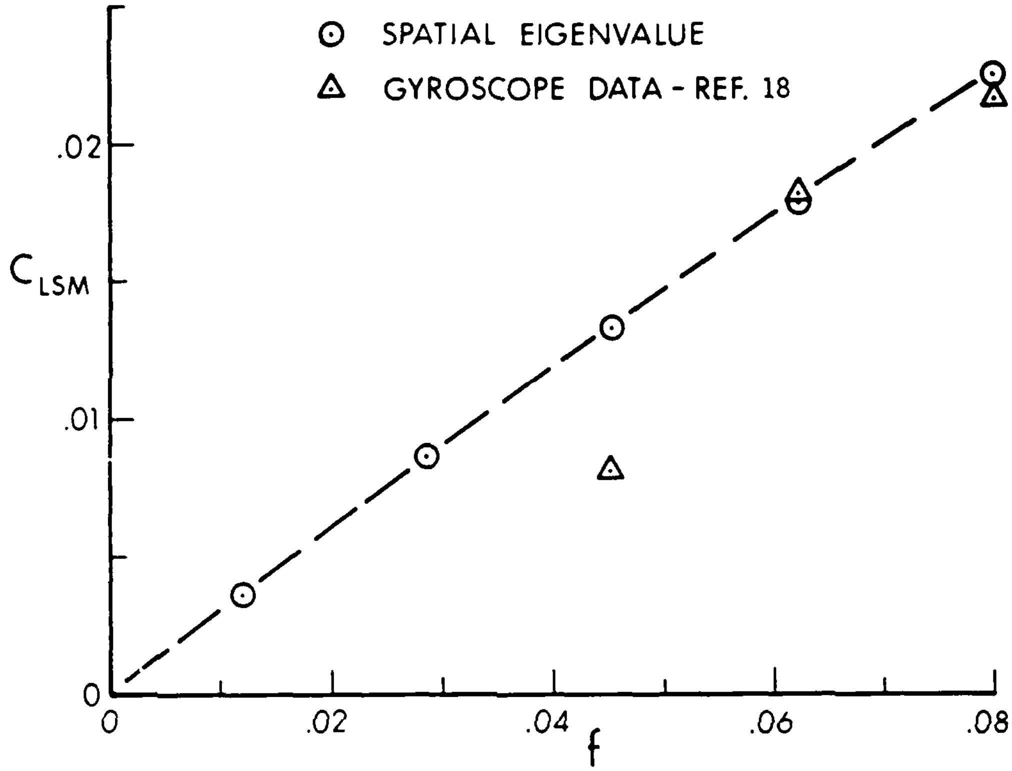

Figure 15. Moment coefficient vs f for Re = 21.5, A = 1.042 according to the spatial eigenvalue method and measurements from Ref. 19 for K_0 = 2°.

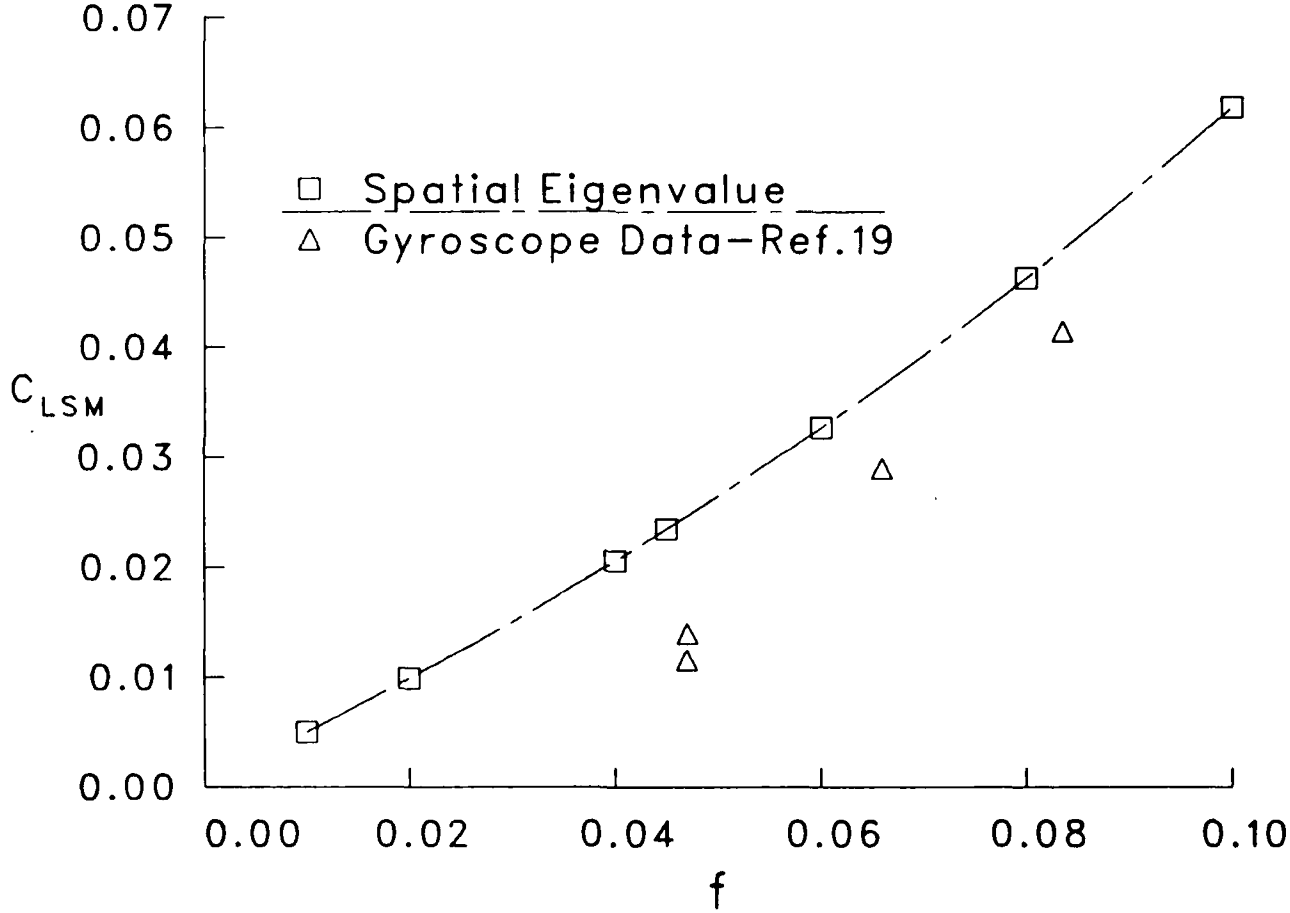

Figure 16. Moment coefficient vs f for Re = 133, A = 1.486 according to the spatial eigenvalue method and measurements from Reference 19 for $K_o = 2°$.

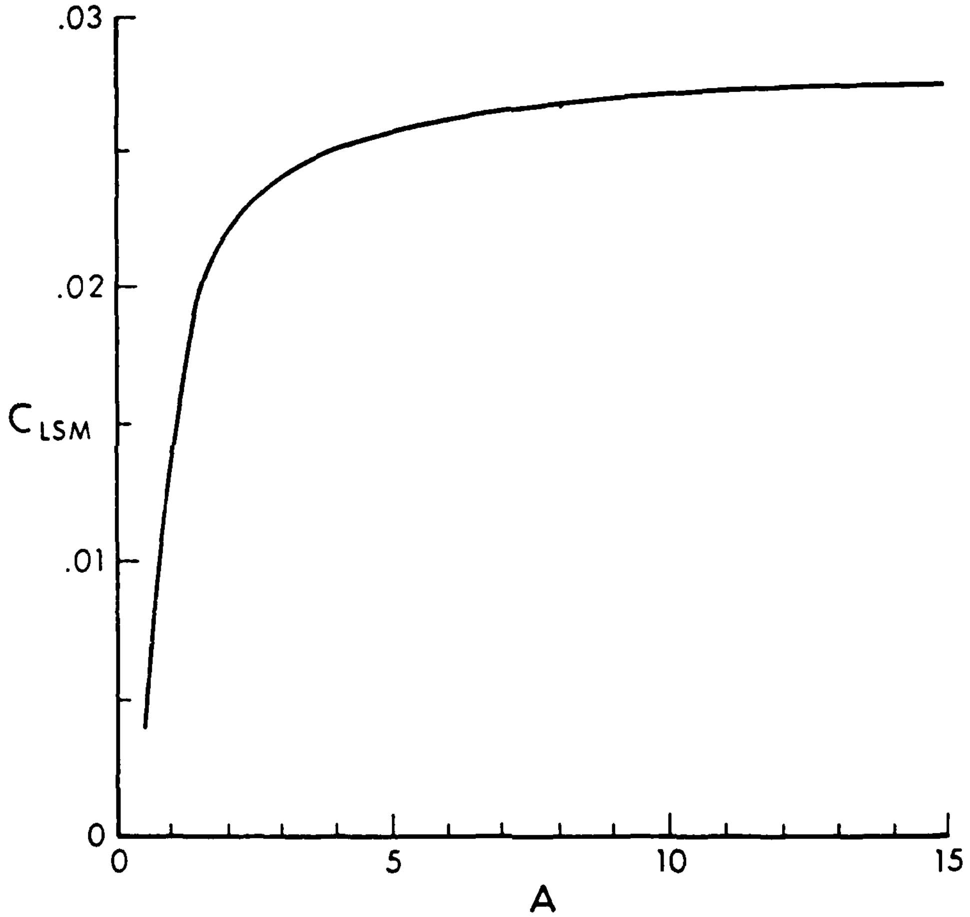

Figure 17. Moment coefficient vs A for Re = 10, f = 0.1, $0.5 \leq A \leq 15$.

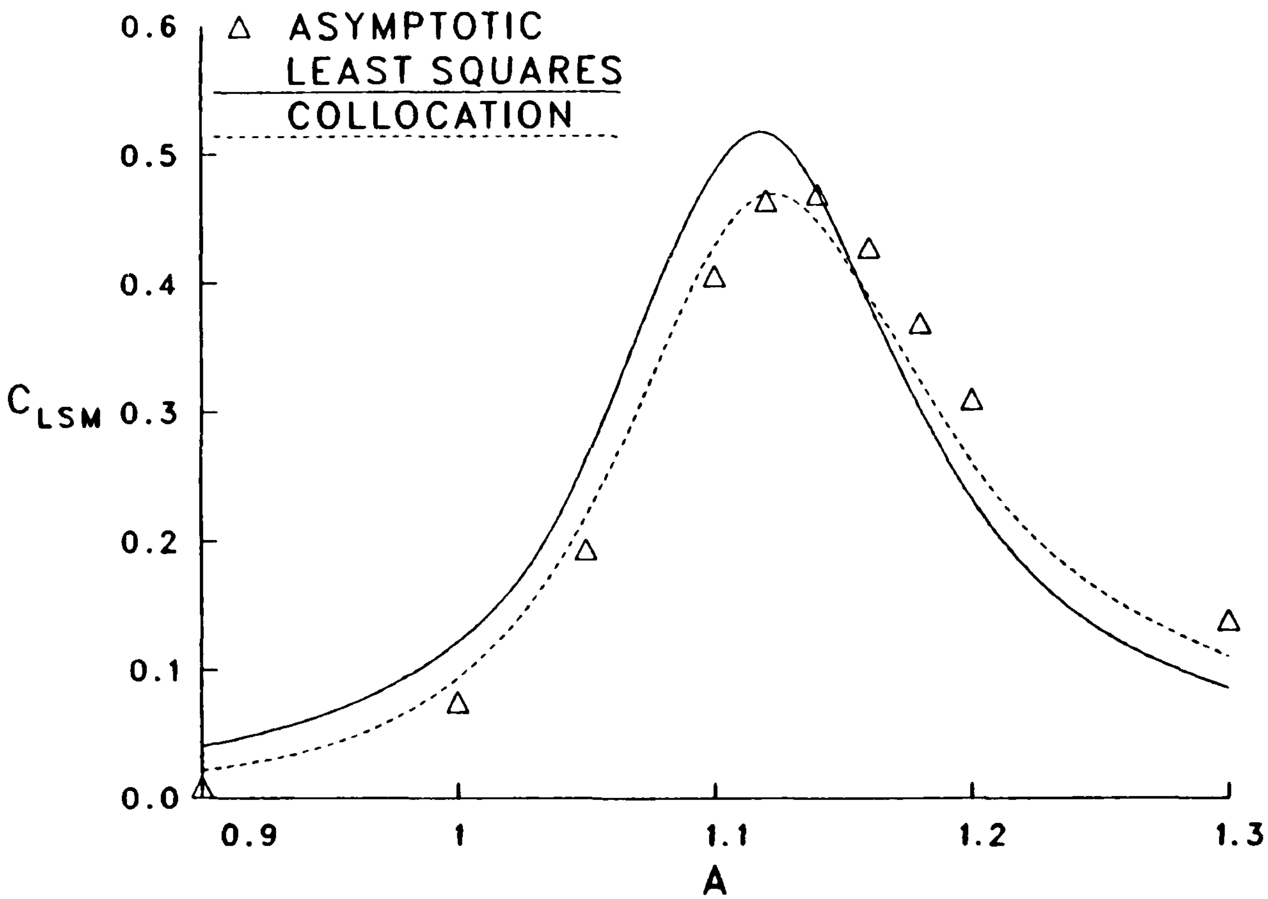

Figure 18. Moment coefficient vs A for Re = 1000, f = 0.1, $0.9 \leq A \leq 1.3$ according to the spatial eigenvalue method using LS and COL and including results according to the asymptotic method of Ref. 4 and 13.

REFERENCES

1. Sedney, R., "A Survey of the Fluid Dynamic Aspects of Liquid-Filled Projectiles," AIAA Paper AIAA-85-1822-CP, AIAA 12th Atmospheric Flight Mechanics Conference, Snowmass, CO., August 1985.

2. Sedney, R., "Some Rotating Fluid Problems in Ballistics," article in Mathematics Applied to Fluid Mechanics and Stability: Proceedings of a Conference Dedicated to Richard C. DiPrima, SIAM, pp. 87-109, Philadelphia, PA., 1986.

3. Herbert, T., "Highly Viscous Fluid Flow in a Spinning and Nutating Cylinder," Second Army Conference on Applied Mathematics and Computing, Army Research Office Report 85-1, Research Triangle Park, NC, May 1984.

4. Gerber, N., Sedney, R., and Bartos, J.M., "Pressure Moment on a Liquid-Filled Projectile: Solid Body Rotation," ARBRL-TR-02422, U.S. Army Ballistic Research Laboratory, Aberdeen Proving Ground, Maryland, October 1982. (AD A120567)

5. Blennerhasset, P.J., and Hall, P., "Centrifugal Instabilities of Circumferential Flow in Finite Cylinders: Linear Theory," Proc. Roy. Soc. London, A-365, pp. 191-207, 1979.

6. Strikwerda, J.C., and Nagel, Y.M., "A Numerical Method for Computing the Flow in Rotating and Coning Fluid-Filled Cylinders," CRDC-SP-85006, 1984 Conference on Chemical Defense Research, Aberdeen Proving Ground, Maryland, November 1984.

7. Nusca, M.J., Private communication, U.S. Army Ballistic Research Laboratory, Aberdeen Proving Ground, Maryland.

8. Sedney, R., and Gerber, N., "A Study of the Critical Layer in a Rotating Liquid Payload," ARBRL-TR-02582, U.S. Army Ballistic Research Laboratory, Aberdeen Proving Ground, Maryland, August 1984. (AD A146094). Also, AIAA Journal, Vol. 23, No. 8, pp. 1179-1184, August 1985.

9. Batchelor, G.K., and Gill, A.E., "Analysis of the Stability of Axisymmetric Jets," Journal of Fluid Mechanics, 14, pp. 529-551, 1962.

10. Davey, A., "A Simple Numerical Method for Solving Orr-Sommerfeld Problems," Quarterly Journal of Mathematics and Applied Mechanics, Vol. 26, Part 4, pp. 401-411, 1973.

11. Kitchens, Jr., C.W., Gerber, N., and Sedney R., "Oscillations of a Liquid in a Rotating Cylinder: Part I. Solid Body Rotation," ARBRL-TR-02081, U.S. Army Ballistic Research Laboratory, Aberdeen Proving Ground, Maryland, June 1978. (AD A057759)

12. Malik, M.R., Chuang, S., and Hussaini, M.Y., "Accurate Numerical Solution of Compressible, Linear Stability Equations," Journal of Applied Mathematics and Physics (ZAMP), Vol. 33, pp. 189-201, March 1982.

REFERENCES (continued)

13. Gerber, N., and Sedney, R., "Moment on a Liquid-Filled Spinning and Nutating Projectile: Solid Body Rotation," ARBRL-TR-02470, U.S. Army Ballistic Research Laboratory, Aberdeen Proving Ground, Maryland, February 1983. (AD A125332)

14. Aldridge, K.D., "Experimental Verification of the Inertial Oscillations of a Fluid in a Cylinder During Spin-Up," ARBRL-CR-273, U.S. Army Ballistic Research Laboratory, Aberdeen Proving Ground, Maryland, September 1975. (AD A018797). Also Geophys. Astrophys. Fluid Dynamics, Vol. 8, pp. 279-301, 1977.

15. Hepner, D.J., Kendall, T.M., Davis, B.S., and Tenly, W.Y., "Pressure Measurements in a Liquid-Filled Cylinder Using a Three-Degree-of-Freedom Flight Simulator," BRL-MR-3560, U.S. Army Ballistic Research Laboratory, Aberdeen Proving Ground, Maryland, December 1986.

16. Vaughn, H.R., Oberkampf, W., and Wolfe, W.R., "Fluid Motion Inside a Spinning Nutating Cylinder," Journal of Fluid Mechanics, Vol. 150, pp. 121-138, 1985. Also "Numerical Solution for a Spinning, Nutating Fluid-Filled Cylinder," Sandia Report SAND 83-1789, December 1983.

17. Murphy, C.H., "Angular Motion of a Spinning Projectile with a Viscous Liquid Payload," ARBRL-MR-03194, August 1982. (AD A118676). Also Journal of Guidance, Control, and Dynamics, Vol. 6, pp. 280-286, July-August 1983.

18. Nusca, M.J. and D'Amico, W.P., "Parametric Study of Low Reynolds Number Precessing/Spinning Incompressible Flows," U.S. Army Ballistic Research Laboratory, Aberdeen Proving Ground, Maryland, BRL Memorandum Report in publication.

19. D'Amico, W.P., "Instabilities of a Gyroscope Produced by Rapidly Rotating, Highly Viscous Liquids," AIAA Paper 81-0224, January 1981. Also, Journal of Guidance, Control, and Dynamics, Vol. 7, No. 4, pp. 443-449, July-August 1984.

20. Rosenblat, S., Private communication, Fluid Dynamics International.

21. Herbert, T., "Spectral Navier-Stokes Solver for the Flow in a Spinning and Nutating Cylinder," paper in publication. Presented at the 1986 Scientific Conference on Chemical Defense Research, Aberdeen Proving Ground, Maryland, November 1986.

APPENDIX. NORMAL EQUATIONS FOR (3.15)

The coefficients, α_n, which minimize $g(\alpha_n)$ in (3.15) are found as the solution of the linear system

$$\sum_{n=1}^{3M} s_{jn}\, \alpha_n = s_j,$$

where $j = 1,\ldots,3M$, $\sigma(r)$ is given by (2.6e), and s_j and s_{jn} are

$$s_j = \int_0^1 \sigma(r)\ \overline{\cot k_j A\ w_j(r)}\ dr$$

$$s_{jn} = \int_0^1 [u_n\, \bar{u}_j + v_n\, \bar{v}_j + \cot k_n A\ \overline{\cot k_j A}\ w_n\, \bar{w}_j]\ dr.$$

DISTRIBUTION LIST

No. of Copies	Organization
12	Administrator Defense Technical Information Center ATTN: DTIC-FDAC Cameron Station, Bldg. 5 Alexandria, VA 22304-6145
1	Commander US Army Materiel Command ATTN: AMCDRA-ST 5001 Eisenhower Avenue Alexandria, VA 22333-0001
1	Commander U.S. Army ARDEC ATTN: SMCAR-TDC Dover, NJ 07801-5001
3	Commander U.S. Armament RD&E Center US Army AMCCOM ATTN: SMCAR-MSI Dover, NJ 07801-5001
1	Commander U.S. Armament RD&E Center US Army AMCCOM ATTN: SMCAR-AET-A Mr. A. Loeb Dover, NJ 07801-5001
1	HQDA DAMA-ART-M Washington, DC 20310
1	Commander US Army Armament, Munitions and Chemical Command ATTN: AMSMC-IMP-L Rock Island, IL 61299-7300
1	Director U.S. AMCCOM ARDEC CCAC Benet Weapons Laboratory ATTN: SMCAR-CCB-TL Watervliet, NY 12189-4050
1	Commander US Army Aviation Systems Command ATTN: AMSAV-ES 4300 Goodfellow Blvd St. Louis, MO 63120-1798
1	Director US Army Aviation Research and Technology Activity Ames Research Center Moffett Field, CA 94035-1099
1	Commander US Army Communications - Electronics Command ATTN: AMSEL-ED Fort Monmouth, NJ 07703-5301
1	Commander CECOM R&D Technical Library ATTN: AMSEL-IM-L, (Reports Section) B.2700 Fort Monmouth, NJ 07703-5000
1	Director US Army Missile and Space Intelligence Center ATTN: AIAMS-YDL Redstone Arsenal, AL 35898-5500
1	AFWL/SUL Kirtland AFB, NM 87117-6008
1	Commander US Army Tank Automotive Command ATTN: AMSTA-TSL Warren, MI 48397-5000
1	Commander US Army Missile Command Research, Development, and Engineering Center ATTN: AMSMI-RD Redstone Arsenal, AL 35898-5230

DISTRIBUTION LIST

No. of Copies	Organization
1	Director US Army TRADOC Analysis Center ATTN: ATOR-TSL White Sands Missile Range, NM 88002-5502
2	Commandant US Army Infantry School ATTN: ATSH-CD-CS-OR Fort Benning, GA 31905-5400
10	C.I.A. OIR/DB/Standard GE-47 HQ Washington, DC 20505
1	Commander US Army Development and Employment Agency ATTN: MODE-ORO Fort Lewis, WA 98433-5000
1	Air Force Armament Laboratory ATTN: AFATL/DLODL Technical Information Center Eglin AFB, FL 32542-5438
1	Air Force Armament Laboratory Aerodynamics Branch ATTN: Mr. Gerald Winchenbach Eglin AFB, FL 32542-5434
1	US Naval Surface Weapons Center M/C K21 ATTN: Dr. Thomas R. Pepitone Dahlgrin, VA 22448
2	Director Sandia National Laboratories ATTN: Dr. W. Oberkampf Mr. W.P. Wolfe Albuquerque,, NM 87185
1	General Electric Company Systems Analysis Manager ATTN: Mr. Robert H. Whyte Lakeside Avenue Burlington, VT 05401

No. of Copies	Organization
1	Commander US Army Jefferson Proving GD ATTN: STEJP-TD-D Madison, IN 47250
2	Commander US Army Research Office ATTN: Dr. R.E. Singleton Dr. Jagdish Chandra P.O. Box 12211 Research Triangle Park, NC 27709-2211
3	Commander Naval Air Systems Command ATTN: AIR-604 Washington, DC 20360
2	Commander David W. Taylor Naval Ship Research & Development Cmd ATTN: H.J. Lugt, Code 1802 S. de los Santos Bethesda, MD 20084-5000
1	Commander Naval Surface Weapons Center ATTN: DX-21, Lib Br Dahlgren, VA 22448
3	Commander Naval Surface Weapons Center Applied Aerodynamics Division ATTN: M. Ciment A.E. Winklemann W.C. Ragsdale Silver Spring, MD 20910
1	Director Office of Naval Research ATTN: Richard Whiting Code 123 800 Quincy Street Arlington, VA 22217

DISTRIBUTION LIST

No. of Copies	Organization
2	AFWAL ATTN: J.S. Shang W.L. Hankey Wright-Patterson AFB, OH 45433
1	Aerospace Corporation Aero-Engineering Subdivision ATTN: Walter F. Reddall El Segundo, CA 90245
5	Director National Aeronautics and Space Administration Ames Research Center ATTN: D.R. Chapman W.C. Rose B. Wick P. Kutler Tech Library Moffett Field, CA 94035
4	Director National Aeronautics and Space Administration Langley Research Center ATTN: E. Price J. South J.R. Sterrett Tech Library Langley Station Hampton, VA 23365
1	Director National Aeronautics and Space Administration Lewis Research Centera ATTN: MS 60-3, Tech Lib 21000 Brookpark Road Cleveland, OH 44135-3127
1	AVCO Systems Division ATTN: B. Reeves 201 Lowell Street Wilmington, MA 01887
2	Director National Aeronautics and Space Administration Marshall Space Flight Center ATTN: A.R. Felix, Chief S&E-AERO-AE Dr. W.W. Fowlis Huntsville, AL 35812
1	Calspan Corporation ATTN: A. Ritter P.O. Box 400 Buffalo, NY 14225
3	Aerospace Corporation ATTN: H. Mirels R.L. Varwig Aerophysics Lab. P.O. Box 92957 Los Angeles, CA 90009
2	Director Jet Propulsion Laboratory ATTN: L.M. Mach Tech Library 4800 Oak Grove Drive Pasadena, CA 91103
3	Arnold Research Org., Inc. ATTN: J.D. Whitfield R.K. Matthews J.C. Adams Arnold AFB, TN 37389
3	Boeing Commercial Airplane Company ATTN: R.A. Day, MS 1W-82 P.E. Rubbert, MS 3N-19 J.D. McLean, MS-3N-19 Seattle, WA 98124

DISTRIBUTION LIST

No. of Copies	Organization	No. of Copies	Organization
2	Lockheed-Georgia Company ATTN: B.H. Little, Jr. G.A. Pounds Dept 72074, Zone 403 86 South Cobb Drive Marietta, GA 30062	1	Northwestern University Department of Engineering Science and Applied Mathematics ATTN: Dr. S.H. Davis Evanston, IL 60201
1	General Dynamics ATTN: Research Lib 2246 P.O. Box 748 Fort Worth, TX 76101	2	Ohio State University Dept of Aeronautical and Astronautical Engineering ATTN: S.L. Petrie O.R. Burggraf Columbus, OH 43210
2	Grumman Aerospace Corporation ATTN: R.E. Melnik L.G. Kaufman Bethpage, NY 11714	2	Polytechnic Institute of New York ATTN: G. Moretti Tech. Library Route 110 Farmingdale, NY 11735
1	Lockheed Missiles and Space Company ATTN: Tech Info Center 3251 Hanover Street Palo Alto, CA 94304	3	Princeton University James Forrestal Research Ctr Gas Dynamics Laboratory ATTN: S.M. Bogdonoff S.I. Cheng Tech Library Princeton, NJ 08540
3	Martin-Marietta Corporation ATTN: S.H. Maslen S.C. Traugott H. Obremski 1450 S. Rolling Road Baltimore, MD 21227	1	Purdue University Thermal Science & Prop Ctr ATTN: Tech Library W. Lafayette, IN 47906
2	McDonnell Douglas Astronautics Corporation ATTN: J. Xerikos H. Tang Cambridge, MA 02139	1	Rensselaer Polytechnic Institute Department of Math Sciences ATTN: Tech Library Troy, NY 12181
2	North Carolina State Univ Mechanical and Aerospace Engineering Department ATTN: F.F. DeJarnette J.C. Williams Raleigh, NC 27607	1	Rutgers University Department of Mechanical, Industrial, and Aerospace Engineering ATTN: R.H. Page New Brunswick, NJ 08903
1	Notre Dame University Department of Aero Engr ATTN: T.J. Mueller South Bend, IN 46556		

DISTRIBUTION LIST

No. of Copies	Organization	No. of Copies	Organization
1	Southern Methodist University Department of Civil and Mechanical Engineering ATTN: R.L. Simpson Dallas, TX 75272	1	University of California - San Diego Department of Aerospace Engineering and Mechanical Engineering Sciences La Jolla, CA 92037
1	Southwest Research Institute Applied Mechanics Reviews 8500 Culebra Road San Antonio, TX 78228	1	University of Santa Clara Department of Physics ATTN: R. Greeley Santa Clara, CA 95053
1	San Diego State University Department of Aerospace Engr and Engineering Mechanics College of Engineering ATTN: K.C. Wang San Diego, CA 92115	1	University of Colorado Department of Astro-Geophysics ATTN: E.R. Benton Boulder, CO 80302
1	Harvard University Division of Engineering and Applied Physics ATTN: G. J. Carrier Cambridge, MA 01238	1	University of Maryland ATTN: W. Melnik College Park, MD 20740
1	Stanford University Dept of Aeronautics/Astronautics ATTN: M. VanDyke Stanford, CA 94305	1	University of Maryland - Baltimore County Department of Mathematics ATTN: Dr. Y.M. Lynn 5401 Wilkens Avenue Baltimore, MD 21228
1	Texas A&M University College of Engineering ATTN: R.H. Page College Station, TX 77843	2	University of Southern California Department of Aerospace Engineering ATTN: T. Maxworthy P. Weidman Los Angeles, CA 90007
1	University of California - Davis ATTN: Dr. Harry A. Dwyer Davis, CA 95616	2	University of Michigan Department of Aeronautical Engineering ATTN: W.W. Wilmarth Tech Library East Engineering Building Ann Arbor, MI 48104
1	University of California - Berkeley Department of Aerospace Engineering ATTN: M. Holt Berkeley, CA 94720		

DISTRIBUTION LIST

No. of Copies	Organization
1	University of California - Santa Barbara Department of Mechanical and Environmental Engineering ATTN: J.P. Vanyo Santa Barbara, CA 93106
4	University of Virginia Department of Mechanical and Aerospace Engineering ATTN: W. G. Wood R. J. Ribando R. Krauss W. E. Scott Charlottesville, VA 22904
1	University of Virginia Department of Mechanical and Aerospace Engineering ATTN: Prof. Ira Jacobson Charlottesville, VA 22904
1	University of Tennessee Department of Physics ATTN: Technical Library Knoxville, TN 37916
1	University of Washington Department of Mechanical Engineering ATTN: Tech Library Seattle, WA 98105
1	University of Wyoming ATTN: D.L. Boyer University Station Laramie, WY 82071
1	University of Wisconsin - Madison Mathematic Research Center ATTN: John C. Strikwerda 610 Walnut Street Madison, WI 53706

No. of Copies	Organization
1	Woods Hole Oceanographic Institute ATTN: J.A. Whitehead Woods Hole, MA 02543
2	Virginia Polytechnic Institute and State University Department Engineering Science and Mechanics ATTN: Tech Library Dr. Thorwald Herbert Blacksburg, VA 24061
1	Fluid Dynamics International ATTN: Dr. Simon Rosenblat 1600 Orrington Avenue Suite 505 Evanston, IL 60201
1	ICASE ATTN: Prof. Philip Hall Mail Stop 132-C NASA Langley Research Center Hampton, VA 23665

Aberdeen Proving Ground

Director, USAMSAA
ATTN: AMXSY-D

Commander, USATECOM
ATTN: AMSTE-SI-F

Commander, CRDC, AMCCOM
ATTN: SMCCR-MU, Mr. W. Dee
ATTN: SMCCR-RSP-A, Mr. M. Miller
ATTN: SMCCR-RSP-A
SMCCR-MU
SMCCR-SPS-IL

USER EVALUATION SHEET/CHANGE OF ADDRESS

This Laboratory undertakes a continuing effort to improve the quality of the reports it publishes. Your comments/answers to the items/questions below will aid us in our efforts.

1. BRL Report Number __________ Date of Report __________

2. Date Report Received __________

3. Does this report satisfy a need? (Comment on purpose, related project, or other area of interest for which the report will be used.) __________

4. How specifically, is the report being used? (Information source, design data, procedure, source of ideas, etc.) __________

5. Has the information in this report led to any quantitative savings as far as man-hours or dollars saved, operating costs avoided or efficiencies achieved, etc? If so, please elaborate. __________

6. General Comments. What do you think should be changed to improve future reports? (Indicate changes to organization, technical content, format, etc.)

CURRENT ADDRESS

Name

Organization

Address

City, State, Zip

7. If indicating a Change of Address or Address Correction, please provide the New or Correct Address in Block 6 above and the Old or Incorrect address below.

OLD ADDRESS

Name

Organization

Address

City, State, Zip

(Remove this sheet, fold as indicated, staple or tape closed, and mail.)

— — — — — — — — — — FOLD HERE — — — — — — — — — —

Director
US Army Ballistic Research Laboratory
ATTN: DRXBR-OD-ST
Aberdeen Proving Ground, MD 21005-5066

NO POSTAGE NECESSARY IF MAILED IN THE UNITED STATES

OFFICIAL BUSINESS

PENALTY FOR PRIVATE USE, $300

BUSINESS REPLY MAIL

FIRST CLASS PERMIT NO 12062 WASHINGTON, DC

POSTAGE WILL BE PAID BY DEPARTMENT OF THE ARMY

Director
US Army Ballistic Research Laboratory
ATTN: DRXBR-OD-ST
Aberdeen Proving Ground, MD 21005-9989

— — — — — — — — — — FOLD HERE — — — — — — — — — —

END
DATE
FILMED
4-88
DTIC